NASA Contractor Report 178323

Breakdown Characteristics of an Isolated Conducting Object in a Uniform Electric Field

by
M. G. Grothaus
T. F. Trost

Report on N.A.S.A. Grant NAG-1-28

December 1986

(NASA-CR-178323) BREAKDOWN CHARACTERISTICS OF AN ISOLATED CONDUCTING OBJECT IN A UNIFORM ELECTRIC FIELD (Texas Technological Univ.) 68 p Avail: NTIS HC A04/MF A01 CSCL 04B G3/47

N87-26490
Unclas
0087620

Department of Electrical Engineering/Computer Science
Texas Tech University
Lubbock, Texas 79409

BREAKDOWN CHARACTERISTICS OF AN ISOLATED CONDUCTING OBJECT IN A UNIFORM ELECTRIC FIELD

by

M. G. Grothaus

T. F. Trost

Department of Electrical Engineering/Computer Science

Texas Tech University

Lubbock, Texas 79409

December, 1986

Prepared for

National Aeronautics and Space Administration

Langley Research Center

Hampton, Virginia 23665

Under Grant No. NAG-1-28

"Lightning Sensors and Data Interpretation"

ABSTRACT

A laboratory experiment has been conducted to determine the physical processes involved in the electrical breakdown of a particular spark gap arrangement. The gap consists of an isolated conducting ellipsoid located midway between two large flat electrodes. Gradual increase of the applied electric field, E, in the gap produces corona on the ellipsoid tips followed by flashover in a leader-arc sequence. The leader phase consists of the abrupt formation of ionized channels which partially bridge the gap and then decay prior to the arc. Measurements of dE/dt and of current were made, and photographs were taken with an image converter camera. Experimental parameters are as follows:

Gap length = 25.4 cm

Ellipsoid length = 10.0 cm

Gap voltage for flashover = 98 kV

Gap electric field strength (far from ellipsoid) = 386 kV/m

Gap capacitance = 78 pF

Gap electric field energy (estimated) = 0.58 J

Peak positive-corona-streamer current = 25 mA

DC corona current = 0.37 - 0.40 mA

Peak arc current = 200 A

Arc channel diameter < 1 mm

Duration of flashover event (leader + arc) ≈ 1 μs

CONTENTS

LIST OF FIGURES iii

SECTION

I. INTRODUCTION 1

Previous Work at Texas Tech 1

New Research at Texas Tech 4

II. EXPERIMENTAL APPARATUS 10

Data Acquisition 11

III. BIPOLAR CORONA 21

Positive Corona 22

Negative Corona 25

IV. FLASHOVER 37

Flashover Characteristics 37

Current Measurement 41

V. CONCLUSIONS 55

REFERENCES 59

APPENDIX 61

LIST OF FIGURES

1. Spark Gap Configurations 6
2. Leader Propagation and Arc Transition in a Positive Point-Plane Gap 7
3. Arc Transition in a Negative Point-Plane Gap 8
4. Leader Propagation and Arc Transition in a Gap Containing an Isolated Conducting Ellipsoid 9
5. Experimental Set-up 15
6. Data Acquisition System 17
7. D-dot Sensor 19
8. I-sensor 20
9. Bipolar Corona 27
10. The Positive Glow Discharge 28
11. Coexistence of Positive Streamers and Positive Glow Corona 29
12. I-sensor Response to Positive Corona Streamers 30
13. I-sensor Response to Individual Positive Corona Streamer 31
14. I-sensor Response to Negative Corona in the Upper Gap 32
15. Negative Corona Discharge 33
16. I-sensor Response to Trichel Pulses with a Positive Glow Discharge Present at the Ellipsoid Anode 34

17. Modulation of the Trichel Pulses when Positive Streamers are Present at the Ellipsoid Anode 35

18. I-sensor Response to an Individual Trichel Pulse 36

19. D-dot Response to Flashover 45

20. The First Pulse of a D-dot Waveform 46

21. Fine-structure in the Leading Edge of the First Pulse of the D-dot Waveform 47

22. Oscillogram of the Extinction Period Preceding Arc Transition 48

23. Transition to Arc 49

24. Color Photo of Flashover 50

25. Integrated D-dot Waveforms of Flashover 51

26. Equivalent Circuit of the Experimental Set-up 53

27. Simultaneous Oscillogram of Both I-sensor and D-dot Sensor Responses to Flashover 54

I. INTRODUCTION

Due to the increased use of composite materials in modern aircraft, on-board digital electronic systems are increasingly susceptable to electrical interference from lightning. In order to provide guidelines for the design and test of future systems which will be immune to this type of disturbance, understanding the actual lightning threat is essential.

In 1980, the National Aeronautics and Space Administration initiated a program for studying the response of aircraft to direct lightning strikes. In-flight lightning measurements were accomplished with an instrumented F-106B Delta Dart aircraft (1). Interpretation of some of the lightning signatures obtained is presented in (2) and (3). Analysis of UHF radar data recorded concurrently with direct strikes to the F-106B suggests that the aircraft actually triggers the strikes (4). In an effort to increase our understanding of the basic physical processes involved, it was decided to investigate a similar type of electrical breakdown phenomenon in the laboratory. As a result, we have constructed a laboratory experiment in which an isolated conducting object triggers the breakdown of a uniform-field spark gap. The gap is stressed by a high-voltage DC power supply.

Previous_Work_at_Texas_Tech

Initial measurements of laboratory spark initiation were accomplished at Texas Tech in 1985 using the three spark gap configurations of Figure 1 (5). These configurations include not only the isolated-object arrangement, which is similar to the aircraft-triggering case, but also the simpler cases of positive and negative point-plane gaps. Data was gathered from a D-dot sensor and an fast framing camera, with the D-dot waveforms being integrated by a 10 μs analog integrator.

Measurement of flashover voltage for the three configurations versus length of the gap was carried out first. The main result was that the flashover voltage in the negative point-plane gap was typically two to three times higher than it was in the positive case as previously observed by Hutzler (6).

A 1.0x10.0-cm aluminum ellipsoid was used as the isolated object in configuration 3, and one-half of this ellipsoid was attached to the underside of the high-voltage electrode in configurations 1 and 2 (Figs. 1a, 1b) to act as the point. The point-plane arrangement allows one to study the breakdown behavior of a single point for comparison with the more complex two-point breakdown of the isolated ellipsoid. The point-plane case may also have some relevance to the aircraft-lightning interaction problem because it is similar to the situation where one lightning channel is already attached to a particular location on the aircraft and then a new channel develops from some other location. The half-ellipsoid together with the entire high-voltage electrode simulate the aircraft, and the high-voltage lead and resistor coming from the power supply simulate the attached lightning channel.

In configuration 1, the plate separation (distance from high-voltage electrode to ground plane) was 21.6 cm (8.5 in) with a power supply voltage of 130 kV. A framing photo for the event is shown in Figure 2. The sequence of five frames is from right to left. The propagation of the leader through the gap was found to be associated with a relatively slow, near-linear rise in the integrated D-dot waveform. When the leader reaches the ground electrode, arc transition occurs, and a sharp increase in the integrated D-dot waveform results (i.e., collapse of the electric field in the gap). The velocity of the leader was found to be 3.3 x 10^4 m/s, which is comparable to that reported by Levesque (7).

For configuration 2, plate separation was 17.1 cm (6.75 in) with a power supply voltage of -168 kV. The framing photo corresponding to this case is shown in Figure 3, with five frames from right to left. Since the event was quite rapid, only the later stages could be seen. The decay of the arc is readily identifiable but no leader propagation prior to the arc is observed.

Configuration 3 was set up by suspending the ellipsoid such that it was oriented vertically in the center of the gap (Figure 1c). The plate separation was 25.4 cm (10 in), and power supply voltage was 152 kV. Note that in this case there were actually two gaps in series, each 7.7 cm in length. The framing photo for the event is shown in Figure 4, with three frames from right to left. The ellipsoid itself is not visible, but it lies in the center between the ionized channels. The completion of a channel in the top gap and partial propagation of a leader across the bottom gap, as shown very faintly in the first frame, resulted in an initial rise in the corresponding integrated D-dot waveform. The closure of the bottom gap and subsequent arc, frames 2 and 3, caused the appearance of a second rise in the integrated D-dot waveform. It is interesting that a leader-arc-transition delay was present and varied in length for different firings. Aging of ellipsoid tips was also observed and was found to have a significant effect on the breakdown voltage of the gap.

New Research at Texas Tech

The focus of present research efforts in our laboratory has turned exclusively to studying the breakdown on an isolated object in a uniform electric field, configuration 3 above. Further understanding of this case requires a more in-depth look at the individual breakdown processes which are involved. An improved experimental arrangement, described in Section II, along with comparisons made with the results reported by other workers, enable us to accomplish this goal.

Bipolar corona was found to have a profound effect on the sequence of events leading to the high current arc, or flashover. As such, Section III explores the basic nature of the corona, which occurs near the tips of the isolated object. Both qualitative and quantitative information is presented for each corona polarity and some of the intrinsic differences which exist between the two are pointed out.

Section IV concentrates on the subject of flashover in the gap. Several preliminary stages of breakdown which necessarily lead to flashover of the gap are revealed through the use of very fast camera techniques and concurrent analysis of sensor waveforms. Direct measurement of peak current in the arc is given as well as an inferred measurement obtained from the response of a D-dot sensor located in the uniform field region.

Conclusions are drawn in Section V along with suggestions related to future research areas which will contribute to continued progress in understanding aircraft-lightning interaction.

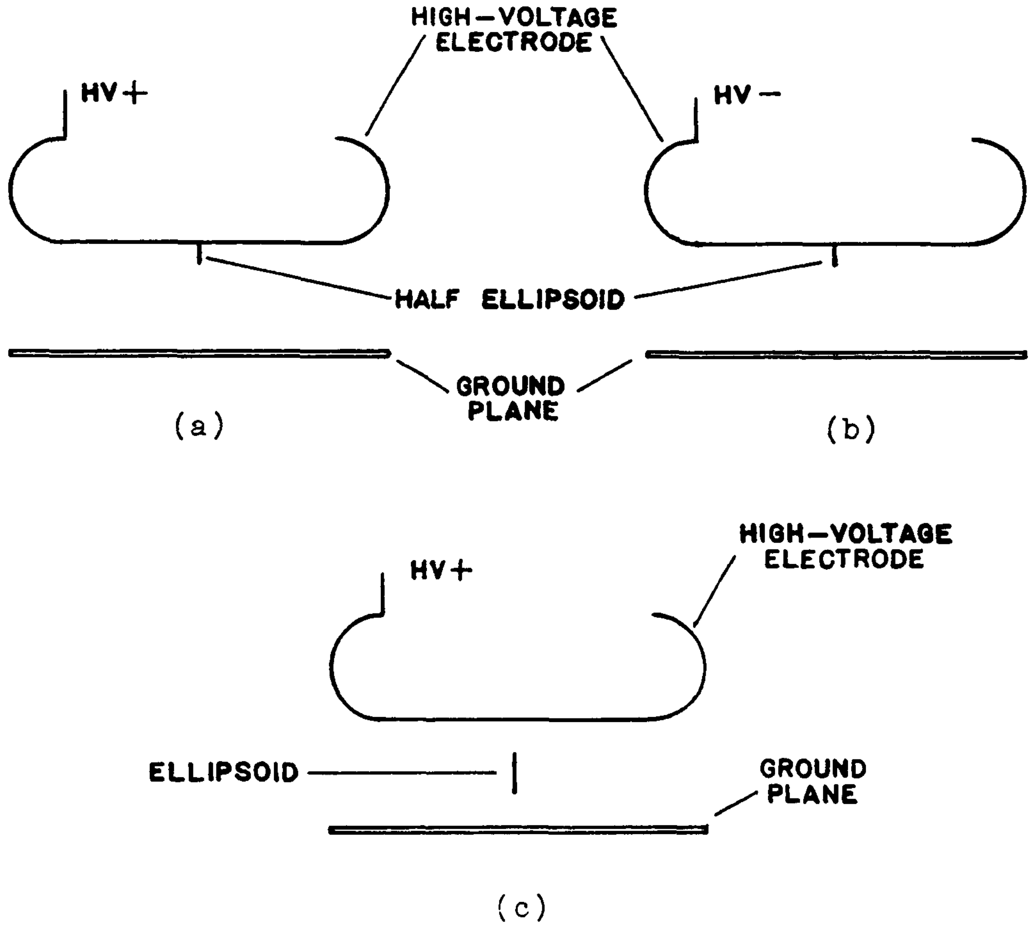

Figure 1: Spark Gap Configurations: (a) Configuration 1: half-ellipsoid attached to positive high-voltage electrode. (b) Configuration 2: half-ellipsoid attached to negative high-voltage electrode. (c) Configuration 3: full ellipsoid centered between positive high-voltage electrode and the ground plane.

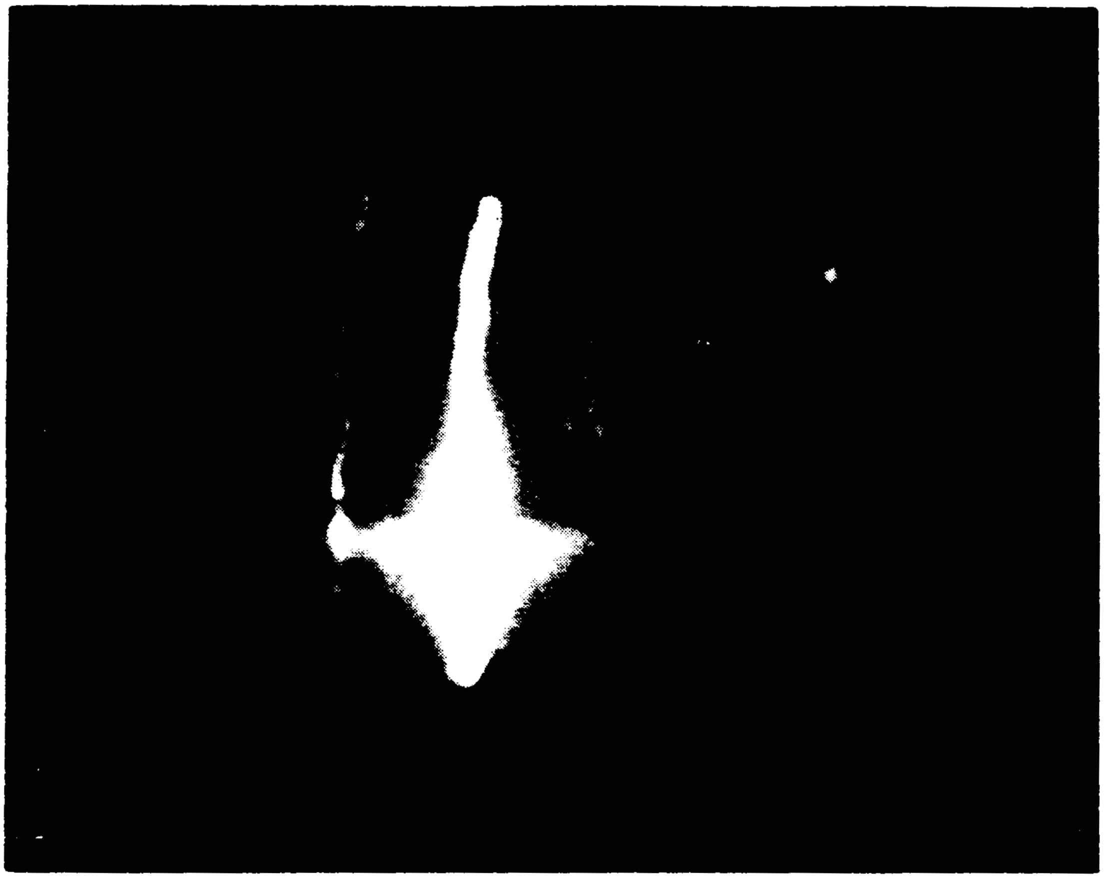

Figure 2: Leader Propagation and Arc Transition in a Positive Point-Plane Gap.

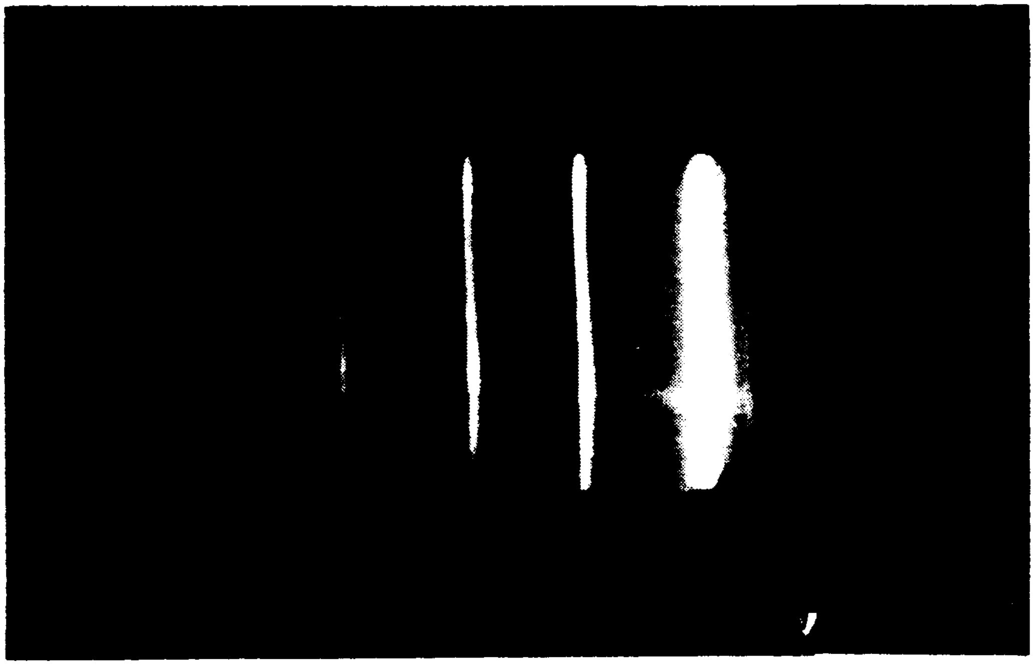

Figure 3: Arc Transition in a Negative Point-Plane Gap.

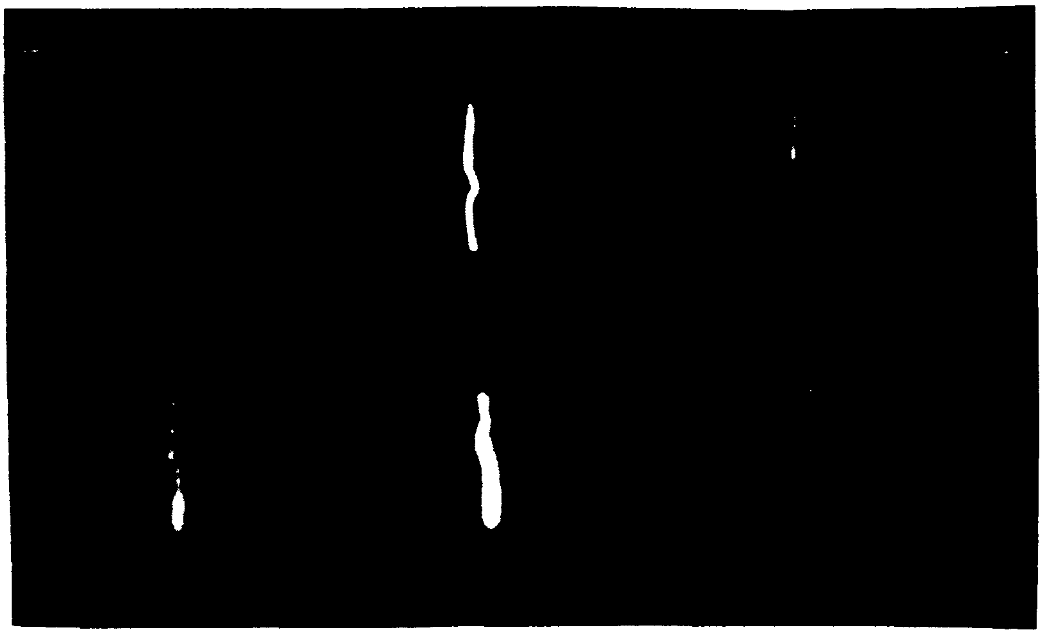

Figure 4: Leader Propagation and Arc Transition in a Gap Containing an Isolated Conducting Ellipsoid.

II. EXPERIMENTAL APPARATUS

The basic experimental setup, a spark gap containing an isolated conducting object in atmospheric air, is shown in Figure 5. An aluminum prolate ellipsoid with a 10.0 cm major axis and a 1.0 cm minor axis is suspended in the parallel plane gap by an adjustable dielectric stand. The ellipsoid represents a field enhancement factor of fifty, roughly approximating that of the F-106B aircraft as discussed in (5). The high-voltage electrode is a 91.4 cm (36 in) diameter aluminum plate with a turned up edge. The large, 12.7 cm (5 in), radius of curvature of the plate's edge tends to limit its observable contribution to the corona current. The ground electrode consists of six 1.2 m x 3.66 m (4 ft x 12 ft) aluminum sheets connected on a steel girder frame to create a 3.66 m x 7.32 m (12 ft x 24 ft) ground plane. Electrode separation is varied by moving the prusik knot on the nylon rope suspending the top plate. With a plate separation of 25.4 cm (10 in), the gap capacitance was measured at 78 pF. Connected across the parallel plate geometry is a Hypotronics model 8000 series 240 kV variable DC power supply with a 4 mA current capability. The supply is equipped with a control unit which displays the output voltage and current on two meters on the front panel. The meters are accurate to within plus or minus two percent full scale. In series with the supply and the high-voltage electrode is a 100 megohm, ±20 %, power resistor. The resistor has corona inhibitors attached to each of its ends and limits the supply current to a maximum of 2.4 mA. The resistor-corona inhibitor geometry produces a capacitance of 26 pF. The output impedance of the power supply was measured to be six megohms and a ripple factor of less than 1 % at full load was observed. These figures of merit indicate that the supply can be considered close to ideal since it is always lightly loaded by the 100 megohm series resistor.

Data Acquisition

The system used for data acquisition is depicted in Figure 6. Data was obtained from two sensors: a D-dot sensor located 48.2 cm (19 in) from the axis of symmetry of the gap and an I-sensor located in-line with the axis. Both sensors are of "flush plate dipole" design in order to minimize field distortion in the gap. The D-dot sensor is a model FPD-1A manufactured by EG&G with a bandwidth of 390 MHz and a sensitivity of 0.01 square meters, and is shown in Figure 7. The I-sensor of Figure 8 was designed and constructed in our lab. It is essentially the same as the EG&G sensor but is connected to a sampling (or shunt) resistor and is used to measure the current flow in the spark. The sampling resistor can be easily changed to give a wide variety of output ranges. If no conduction current contacts the I-sensor, then it operates as a D-dot sensor. The dimensions of the sensor were chosen to give the desired bandwidth and sensitivity in accordance with the results of (8), (9) and (10). Using a Tektronix type 7S12 Time Domain Reflectometer (TDR), the sensor risetime, with no sampling resistor, was found to be 0.09 ns, giving a bandwidth of 390 MHz. Using a sampling resistor, and thus reducing the load resistance, results in a larger bandwidth due to the RC-dependence of the risetime. The sensitivity of the sensor is 0.015 square meters.

The sensors are connected to a Tektronix 7834 mainframe storage oscilloscope with two 2.74 m (9 ft) sections of 50 ohm semi-rigid coaxial cable and Type N coaxial connectors. The plug-ins used with the scope are a Tektronix type 7A26 dual-channel amplifier with 200 MHz bandwidth and a Tektronix type 7B53A time base. A single scope trace of the outputs of the two sensors is accomplished by delaying one of the sensor signals with respect to the other and setting the scope to the add mode. The delay was obtained by connecting a 250 ns delay line (with 3.68 dB attenuation) to one of the input channels on the 7A26.

In addition to oscillograms of the sensor signals, photographic data was obtained with a TRW model 1D Image Converter Camera complete with a model 6B high speed framing plug-in. Exposure times are 20 ns and interframe delay is 50 ns. The 300 volt pulse required to trigger the camera is provided by a TRW model 46A Trigger Delay Generator (TDG) at a risetime of 10 ns. The 50 ohm trigger input of the TDG is driven by a high-speed JFET source follower amplifier connected to the gate output of the oscilloscope. Unfortunately, the time between trigger input to the TDG and the "zero-delay" output from the TDG is 115 ns, so that this amount of delay is always present before the first camera frame. The scope is externally triggered by the signal from the D-dot sensor. Additional visible-light photographic data was obtained through the use of a Pentax K1000 35 mm camera with a 75 to 200 mm Albinar zoom lens and ASA 200 Kodacolor film.

To provide relative immunity to the effects of electromagnetic interference from the discharge in the gap, the scope and trigger generating components were located in a screen box. In addition, the AC power strip inside the box was filtered. Appropriate attenuation of sensor signals was provided by Narda (DC-3 GHz, 0.3 kW peak) 20 dB attenuators and a Weinschel (5 kW peak) 20 dB attenuator.

THIS PAGE INTENSIONALLY LEFT BLANK

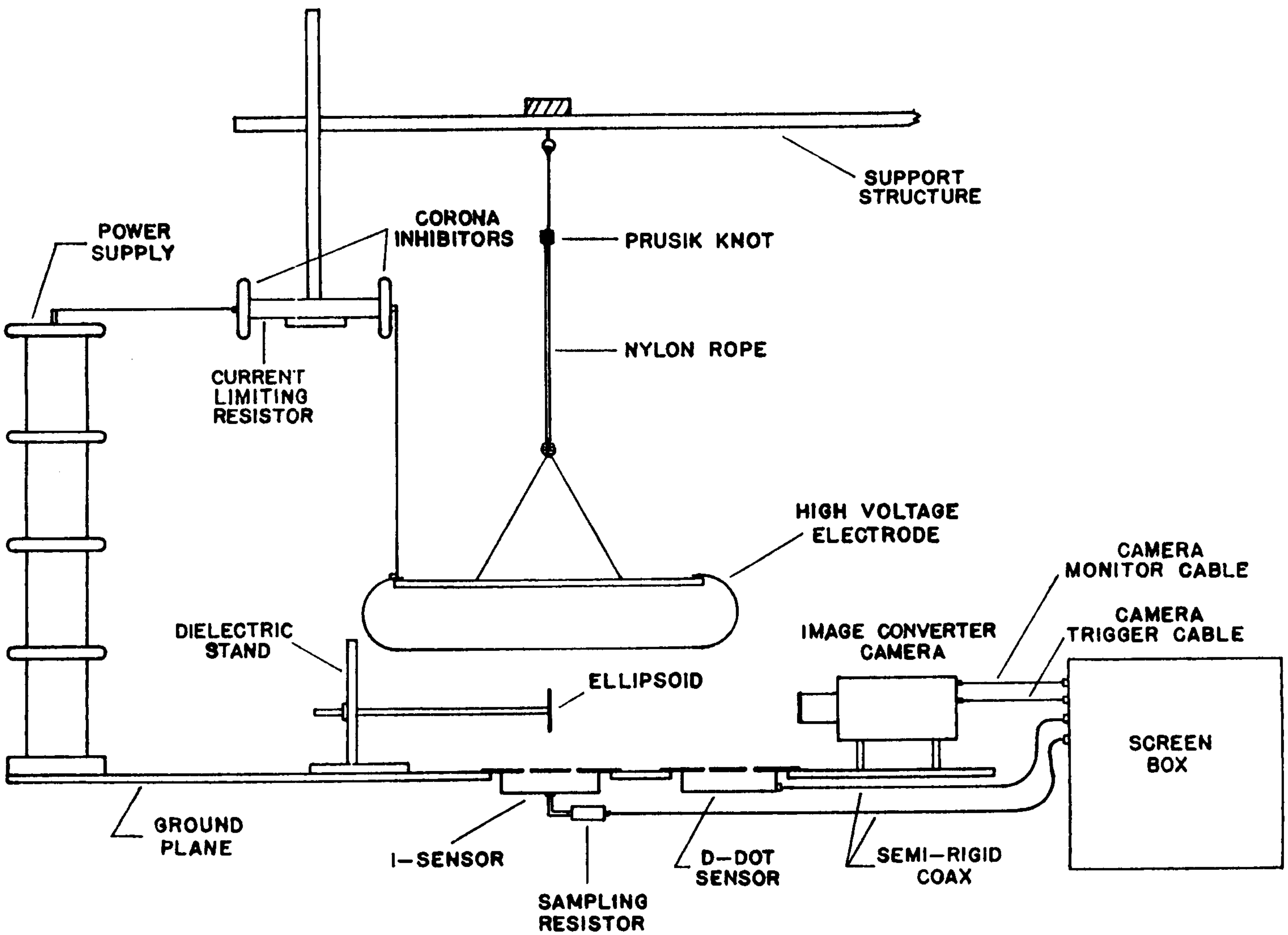

Figure 5: Experimental Set-up

THIS PAGE INTENSIONALLY LEFT BLANK

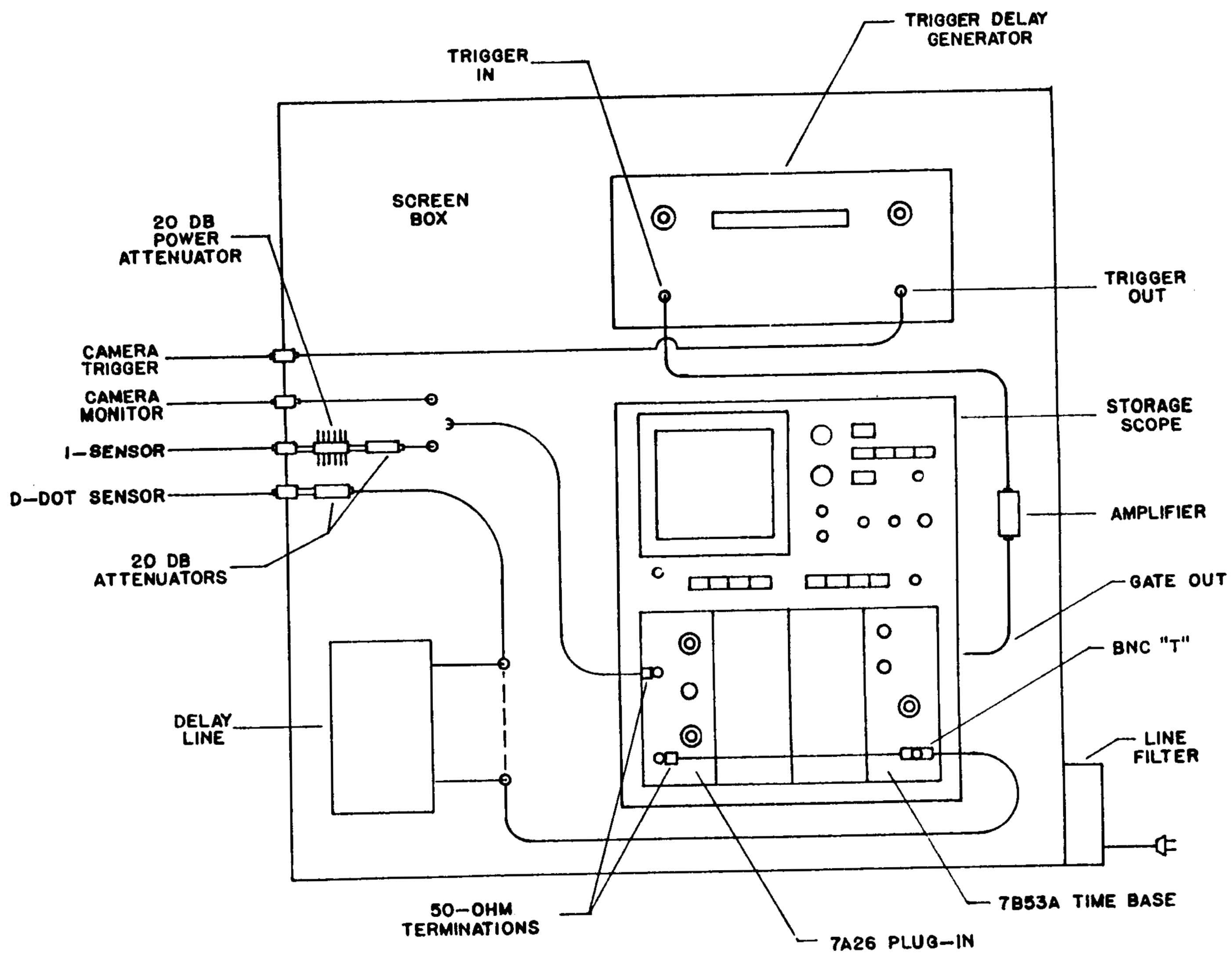

Figure 6: Data Acquisition System

THIS PAGE INTENSIONALLY LEFT BLANK

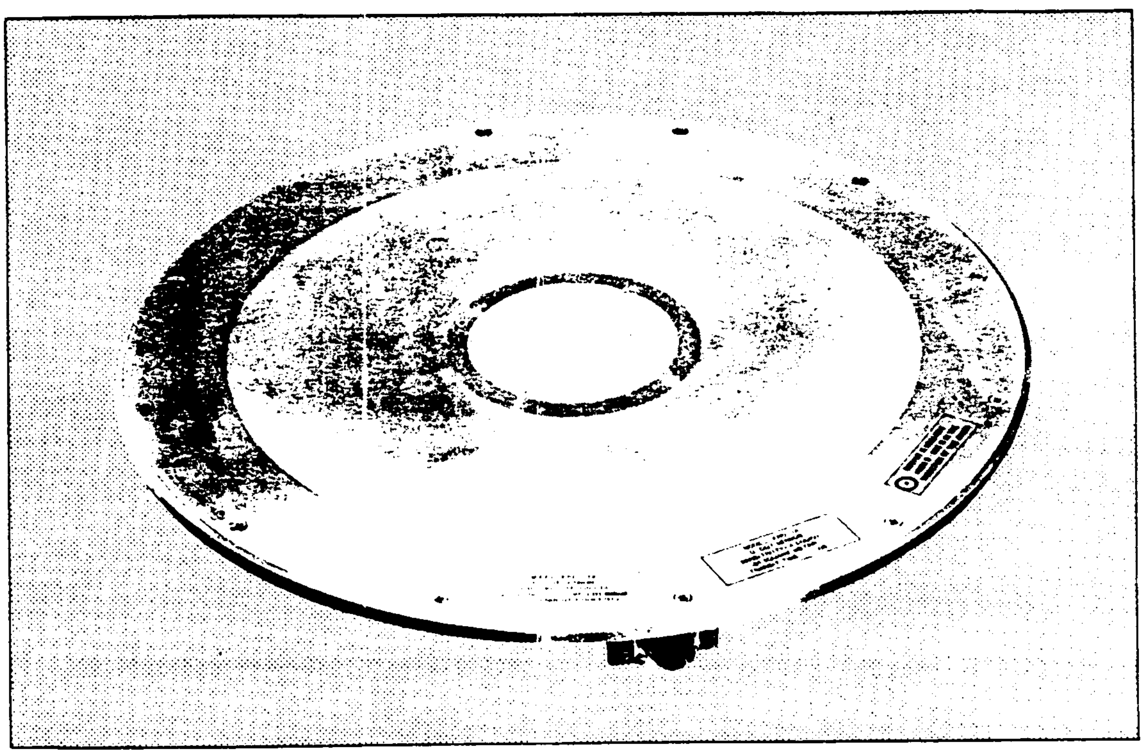

Figure 7: D-dot Sensor (Photo courtesy EG&G Inc.)

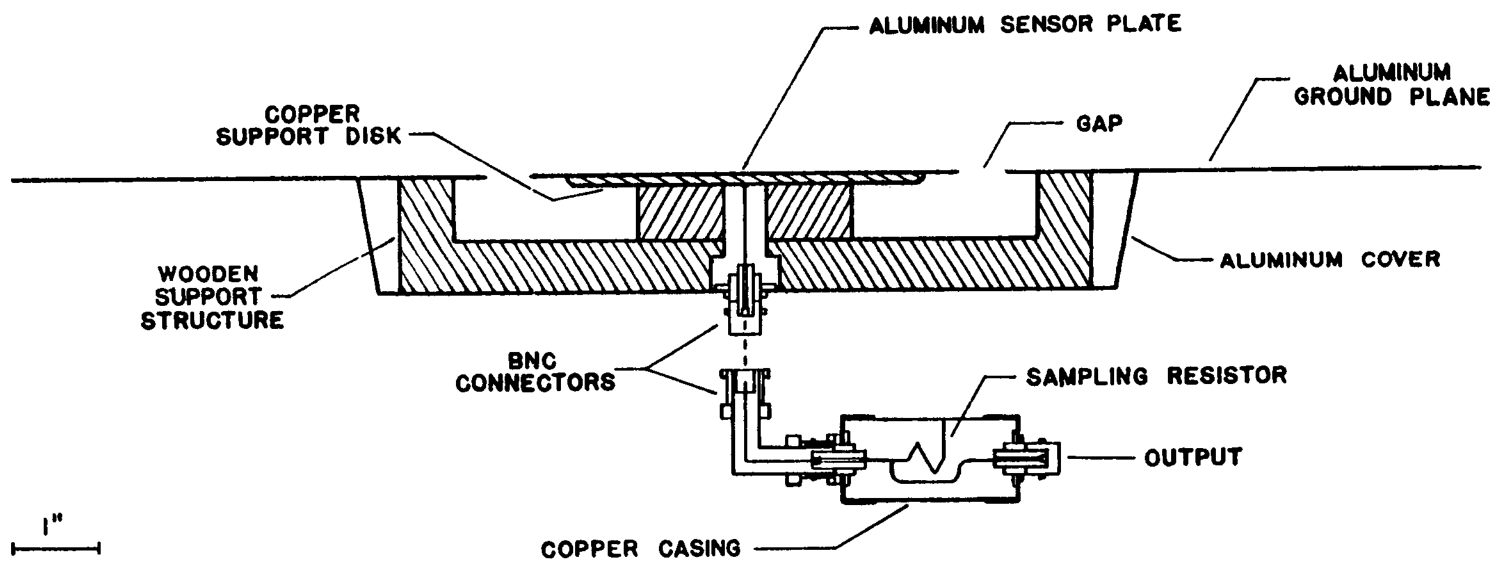

Figure 8: I-sensor

III. BIPOLAR CORONA

Due to enhancement of the local electric field near the ellipsoid, visual manifestations of ionization and excitation processes, known as "partial breakdown" or coronas, can be observed and studied long before complete breakdown of the gap. These coronas will be bipolar in nature, i.e., emanating from both the positive and negative tips of the ellipsoid (Figure 9a). For the positive high-voltage case, the ellipsoid takes on the polarities shown in Figure 9b, with negative corona appearing in the top gap and positive corona in the bottom gap. Keeping in mind the symmetry resulting from the two flat plates, reversal of the ambient field yields the same phenomena with the locations of the positive and negative coronas being transposed (Figure 9c).

Application of a DC voltage to the high-voltage electrode, rather than a pulsed voltage, will allow accumulation of space charge near the ellipsoid tips which can assume a transient or a stationary form. If conditions are such that this space charge becomes stable, considerable distortion of the original "point-plane" fields of the upper and lower gaps will occur, resulting in the appearance of different corona modes.

Positive and negative coronas exhibit remarkably different characteristics and will therefore be treated individually in the following sections. Since we are primarily concerned with conditions conducive to complete breakdown of the gap, we will focus our attention on corona at voltages slightly below breakdown potential for the gap. In this situation the DC corona current, as measured by the panel meter on the power supply, is in the range 0.37 to 0.40 mA.

Positive Corona

We have observed two distinct modes of positive corona. The first mode, henceforth referred to as glow corona, consists of a thin region near the positive tip (anode) of the ellipsoid. The steady glow occurs when sufficient space charge of negative ions accumulates around the anode (11). A quasi-uniform field is set up between this space charge and the anode, as shown in Figure 10. If the space charge is of ample density, the locally confined field will be large enough to cause "breakdown" in this gap. Because of the quasi-uniform nature of the field, this breakdown is Townsend with photoionization of the gas as the main source of the secondary electrons (11). As the voltage on the high-voltage electrode is increased, another mode of corona appears in the form of a pre-breakdown streamer. This mode develops from the glow when the field is adequately non-uniform. Glow corona may exist simultaneously with the streamers as seen in Figure 11. In this photograph, the glow is recognized as the bright region near the tip of the ellipsoid (top) and the streamers are the readily apparent blue column extending far into the gap and eventually contacting the gap electrode.

With the I-sensor mounted in the ground plane directly beneath the ellipsoid, as previously described in Section II, several oscillograms of positive streamer activity were recorded. A typical trace, for an ambient electric field of 3.86 kV/cm*, is shown in Figure 12. The positive polarity of the pulses indicates that positive charge is flowing from the sensor plate through the sampling resistor to ground, as it must for downward streamer currents. The frequency of the pulses was typically found to be 20 to 30 kHz and was, for the most part, regular, with slight variations in pulse amplitude.

A closer look at the structure of the individual pulses yields the waveform of Figure 13. From this figure, we can see that the record consists of five distinct regions: an initial flat region of very small amplitude, a steeply rising front and associated current peak, a decay, a steady current which may flow for varying lengths of time, and, finally, a second current peak and eventual decay to zero. Recalling that the sensor behaves like a D-dot sensor until the streamers make actual contact with the sensor plate (at which time the record represents conduction current), the uniform propagation of a streamer from the anode should be associated with a constant D-dot level for approximately 150 ns. The tail end of this response is seen as the flat region of minute amplitude at the extreme left of the waveform. The

----

*This field value is obtained by dividing gap voltage by gap length. The gap voltage equals the power supply voltage (read from panel meter) minus the drop in the 100 megohm resistor due to the DC corona current (read from panel meter).

sharp rise in the leading edge of the waveform should correspond to the bridging of the gap by the streamer. The linking of the ellipsoid anode and the sensor by the streamer produces a current maximum of typically 25 mA. The positive streamer current then decays to a level determined by the electron attachment coefficient, v, for air ($v = 10^6/s$). The current flowing after this decay, about 10 mA, is referred to as a "dark current" and is probably due to electrons generated within the channel itself, some detachment process, or contribution from the cathode (12). This dark current, which flows through the low conductivity channel of the bottom gap (about 3 megohms/cm as measured by Bicknell (12)), seeks to charge up the capacitance of the "point-plane" geometry in the top gap. The capacitance, estimated at 1 pF, would have a charging time of about 23 μs, accounting for the flatness of the current waveform in this region. However, a second current peak occurs which cuts short this charging process and leads to the immediate decay of the current. The appearance of the second current maximum creates a waveform which appears somewhat similar to the two-peak signature of the flashover described in the next section. In the present case, the second peak may be due to some phenomenon occurring in the top gap or to increased ionization in the lower gap causing a rise in the conductivity of the channel. Unfortunately, no image converter photos are available of this event.

Further increase in the sensitivity of the scope trace shows evidence of a fine-structure contained in the waveform of

Figure 12. This fine-structure is illustrated in the oscillogram of Figure 14. The pulses represent the D-dot response of the sensor to negative corona in the upper gap.

Negative Corona

Unlike the positive corona, the observed negative corona remained completely localized (Figure 15). The solid angle encompassed by the corona increases with increasing ambient field. In order to enhance the sensitivity of the I-sensor to the negative corona, the high-voltage electrode was made negative, thus producing the negative corona in the bottom gap. Oscillograms show that the negative corona consists of the usual characteristic Trichel pulses. No negative glow mode was observed.

When a positive glow is present at the ellipsoid anode, the Trichel pulses are regular with a frequency of approximately 60 kHz (Figure 16). The frequency of the Trichel pulses depends on the time needed to clear the gap of the negative ions produced in the previous pulse (13). Figure 17 illustrates the case when positive streamers are present at the anode. The D-dot response of the sensor to these streamers is marked by the larger periodic pulses in the oscillogram, and the Trichel pulses are the fine-structure in between. The Trichel pulses show marked frequency and amplitude modulation as previously noted by Bicknell (14) whose experiment, using an isolated conducting cylinder, was similar to ours. In the present case, the pulses exhibit a frequency ranging between 150 and 400 kHz.

Examining the individual Trichel pulses more closely, we obtain the waveform of Figure 18. The pulse consists of a quick rise to a D-dot maximum and then a decay to zero. Pulse width was roughly 150 ns.

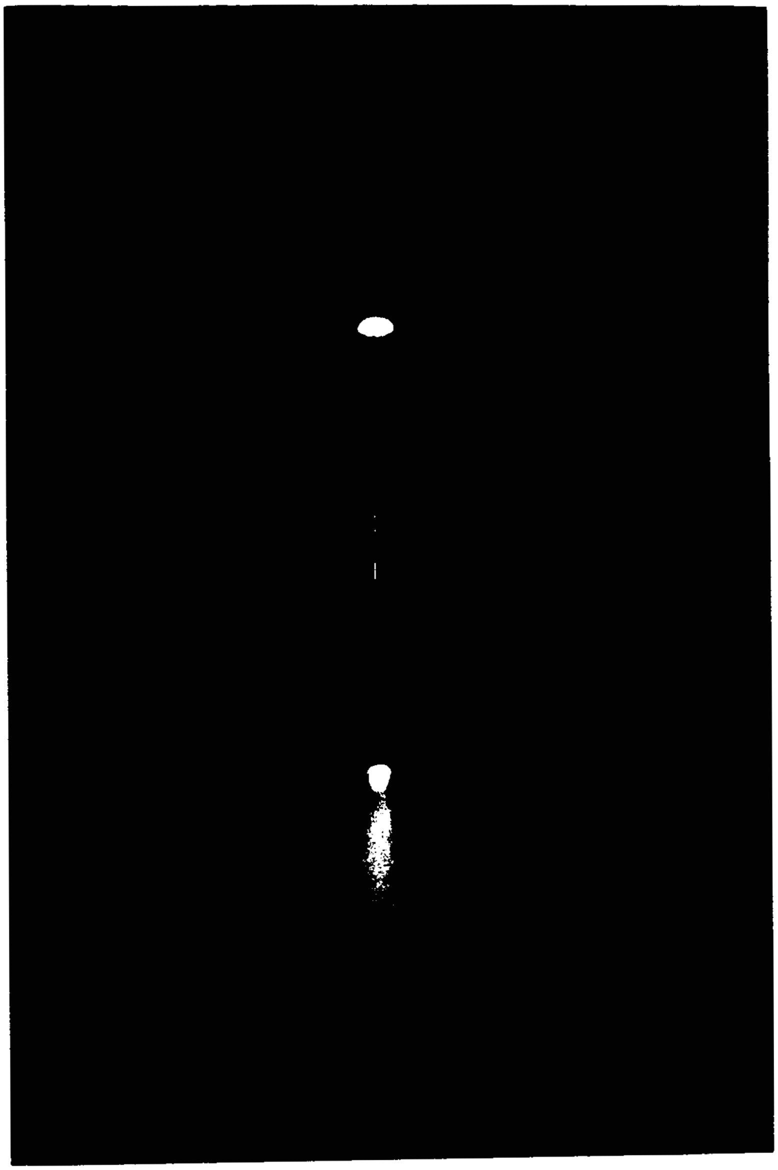

(a)

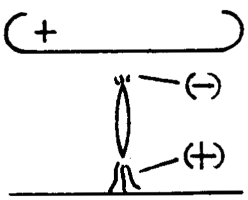

(b)

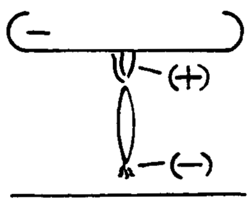

(c)

Figure 9: Bipolar Corona: (a) Bipolar corona emanating from the ellipsoid tips. (b) Corona polarities for positive high-voltage electrode case. (c) Corona polarities for negative high-voltage electrode case.

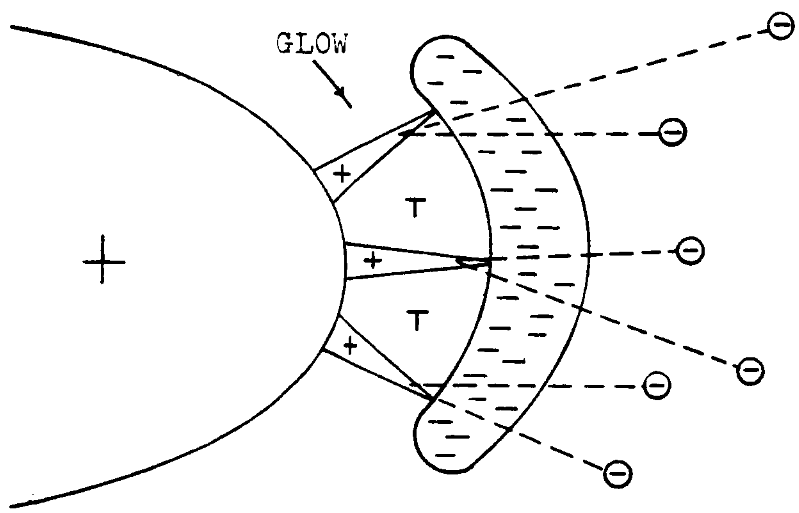

Figure 10: The Positive Glow Discharge

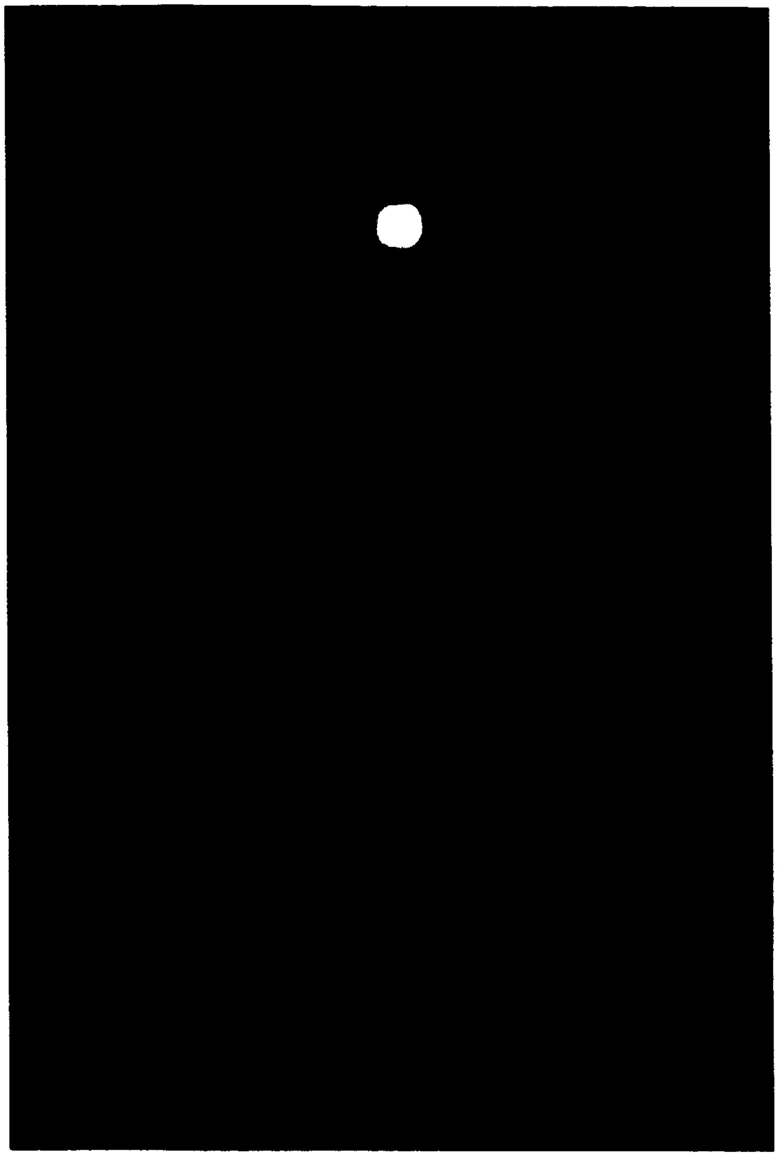

Figure 11: Coexistence of Positive Streamers and Positive Glow Corona.

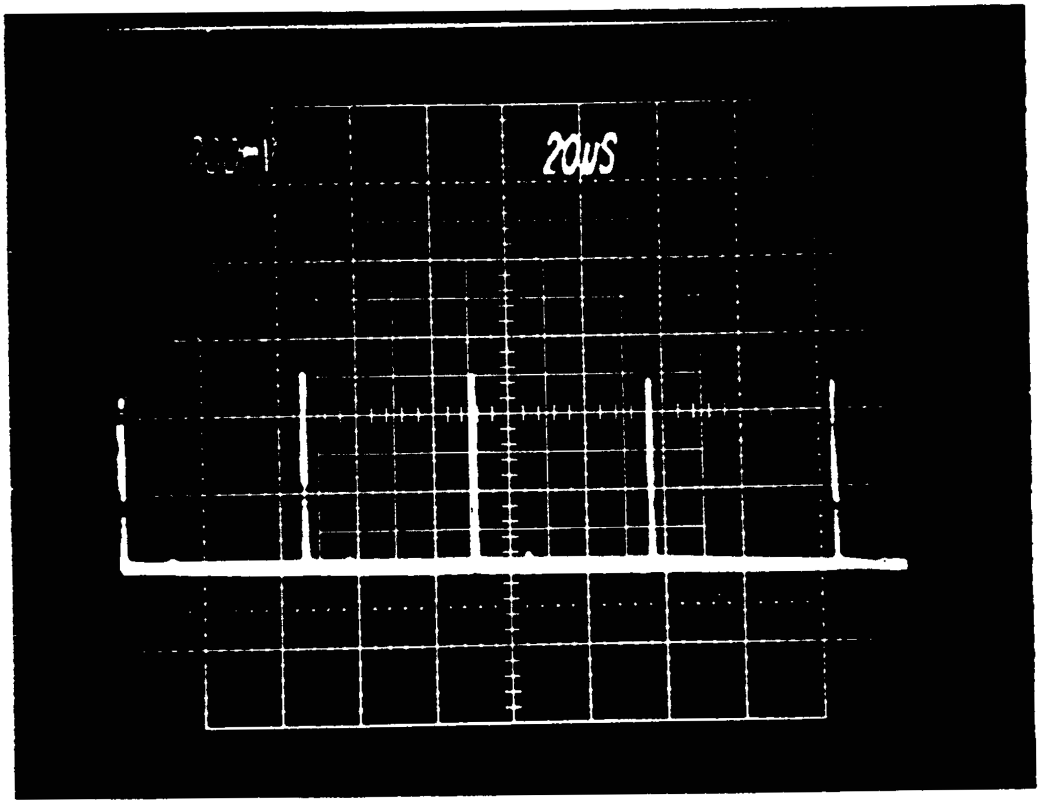

Figure 12: I-sensor Response to Positive Corona Streamers.

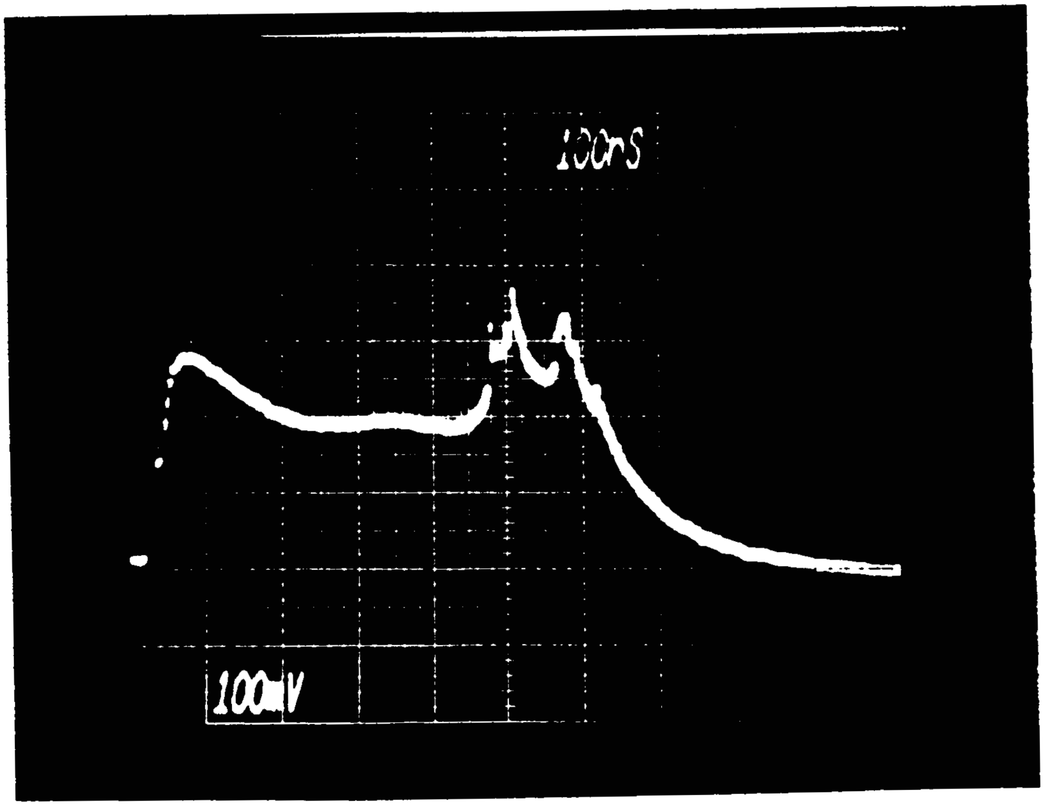

Figure 13: I-sensor Response to an Individual Positive Corona Streamer.

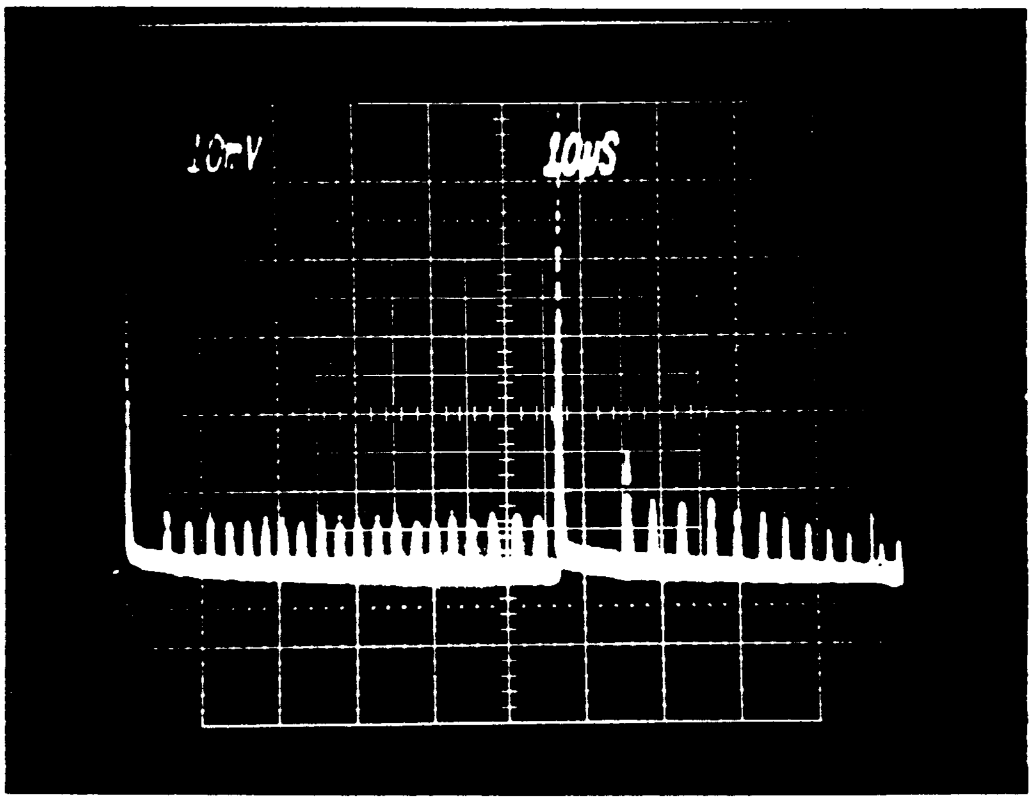

Figure 14: I-sensor Response to Negative Corona in the Upper Gap.

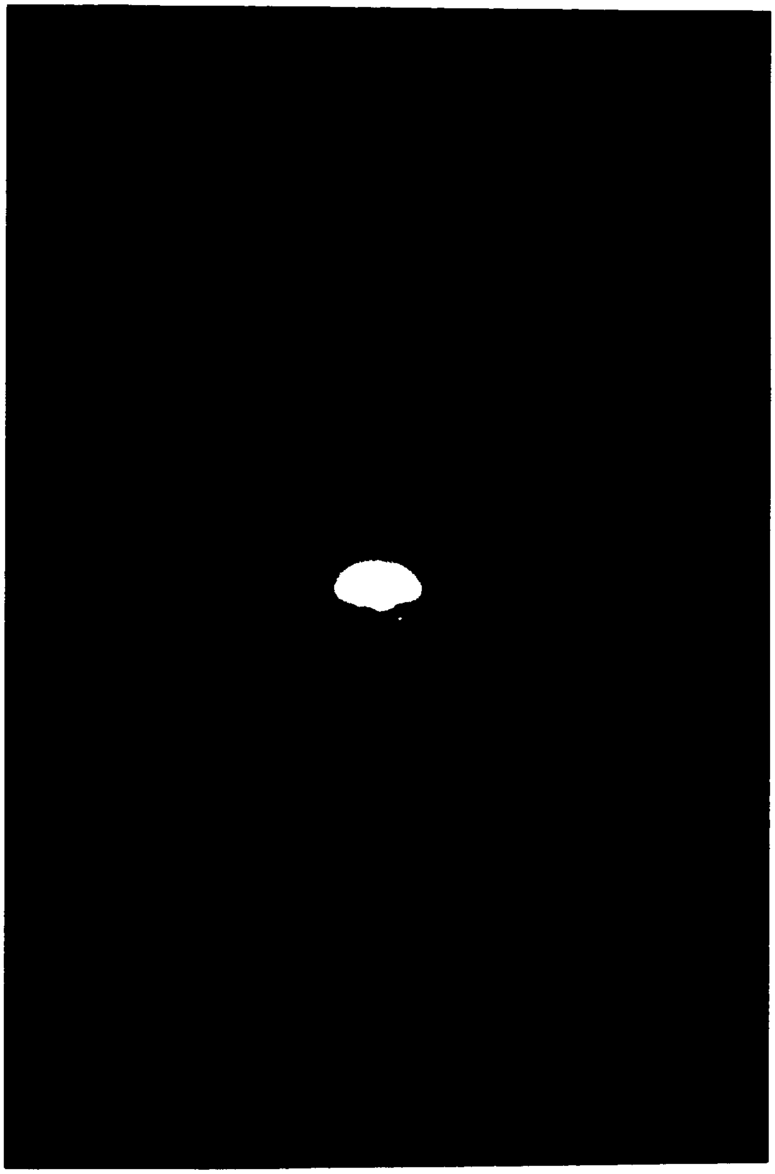

Figure 15: Negative Corona Discharge

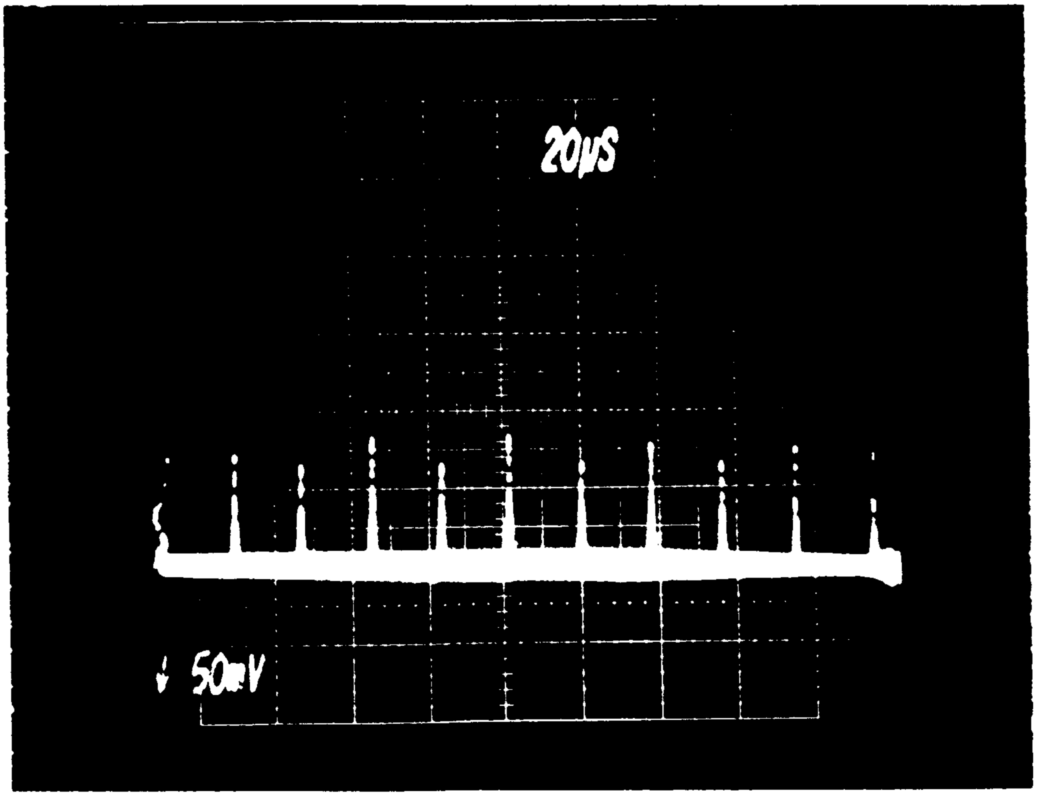

Figure 16: I-sensor Response to Trichel Pulses with a Positive Glow Discharge Present at the Ellipsoid Anode.

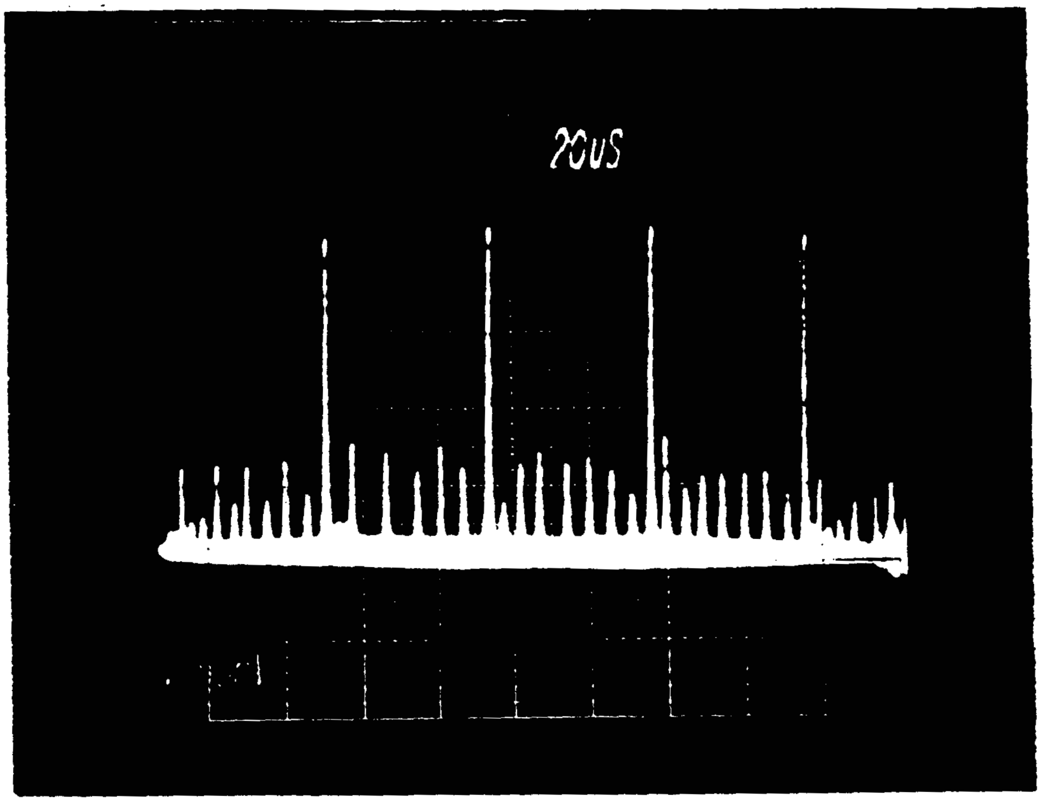

Figure 17: Modulation of the Trichel Pulses when Positive Streamers are Present at the Ellipsoid Anode.

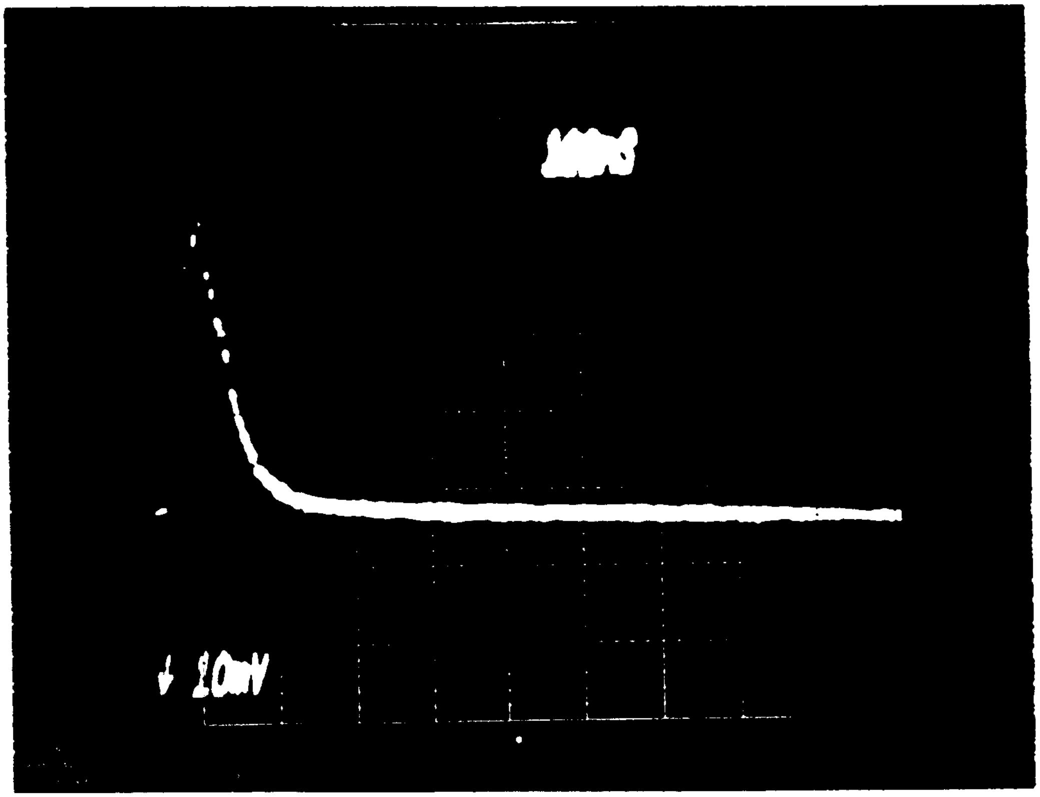

Figure 18: I-sensor Response to an Individual Trichel Pulse.

IV. FLASHOVER

Having discussed partial breakdown, attention will now be turned to the high current phenomenon of complete breakdown of the gap, namely flashover. High speed photographic data and recorded sensor responses are correlated in order to develop a scenario for the flashover process. In addition, two methods of arc current measurement will be presented and compared. The required power supply voltage is 136 kV.

Flashover Characteristics

A representative waveform obtained from the D-dot sensor during flashover is shown in Figure 19. The waveform is composed of three distinct parts: an initial pulse of roughly 350 ns duration, a time delay which may be of widely varying length and is nonexistent in Figure 19, and a second intense pulse of 40 to 50 ns width. Correlation of the image converter camera photographs with the D-dot waveforms is achieved by superimposing the camera monitor pulses on the waveform.

Investigation of the first pulse of the D-dot waveform proved to be a very difficult problem. Since the experiment involved DC voltages and relied on the spontaneous occurrence of flashover rather than a triggered occurrence, the time delays inherent in the diagnostic system prevented us from photographing the discharge during the initial rise of the first pulse in the D-dot waveform. Various techniques were employed to reduce this "event-to-photo" delay as discussed in the Appendix. Despite this limitation, information about the latter part of the first pulse was obtained. Figure 20a shows an oscillogram of the first pulse of the D-dot waveform. The corresponding framing photo was quite faint so a representative drawing of the results is given instead of the actual photo (Figure 20b). From this figure, the following can be observed:

(a) The camera monitor pulses indicate that the first frame of the photo coincides very nearly with the maximum of the waveform shown. At this point, a leader has already formed across the top gap and a leader, with its associated corona bush tip, is partially bridging the bottom gap. The fact that the negative "point-plane" (top) gap breaks first is interesting in that, as previously noted, it takes two to three times the voltage to break a negative point-plane gap as it does to break its positive counterpart. In our case, the presence of the relatively conductive corona streamers in the lower gap effectively lowers the acquired potential of the ellipsoid, thus increasing the field strength in the top gap, causing it to break first. This dominance of the early stage of breakdown by the negative point-plane gap is further illustrated by moving the ellipsoid down from the midplane of the gap towards the ground plane. The larger the negative point-plane separation, the larger the required power supply potential for flashover. Framing photos showing negative leader propagation were not obtained due to the extremely high speed of closure of the top gap; thus we do not know precisely where within the top gap the leader began. Some fine structure is evident in the leading edge of a few of the acquired D-dot waveforms, as illustrated by Figure 21.

(b) The second frame shows a decay in the luminosity of the established channel. The completion of a channel in the top gap leads to the appearance of a high electric field in the bottom gap, causing a positive leader to propagate towards the I-sensor. The upper channel, not having made the transition to the high conductivity conditions required for the high current arc, is still of relatively low conductivity. Consequently, the current drawn across the high impedance of the top gap by the positive leader in the bottom gap precipitates a drop in the potential of the ellipsoid and extinction of the positive leader. This relaxation type of extinction phenomenon has been previously observed by Labaune (15).

(c) The third frame indicates complete loss of luminosity by the channel and a corresponding decay in the D-dot waveform. This marks the beginning of a period of extinction (typically less than 1 μs) preceding the actual transition to arc. The oscillogram of Figure 22 is typical of those obtained in this period and the related framing photo (not shown) gives no real evidence of luminosity in the gap.

The transition to arc of the entire gap is marked by the second pulse of the D-dot waveform. A D-dot oscillogram is illustrated in Figure 23a with its corresponding framing photo given in Figure 23b. The first frame shows no luminosity since it occurs in the period of extinction. In the second frame, however, visible evidence of activity in the gaps is readily apparent. A very faint reillumination of the channel in the upper gap is present, but, as can be seen, the transition to spark occurs first in the bottom gap. This identification of the actual location of the beginnings of the arc with a framing photo has not been reported by previous workers. A time exposure photograph of the entire arc events given in Figure 24.

For the event of Figure 23, arc transition occurs without being preceded by leader propagation from the positive point of the lower gap. In some instances, however, there is evidence that indicates that positive leader propagation does precede arc transition. Figure 25 consists of two integrated D-dot waveforms of separate events. Aside from the decays due to the time constants of the analog integrators used, the waveforms provide a picture of the collapse of the electric field in the gap. Comparing the two waveforms, we see that the upper is a relatively short event while the lower is quite a bit longer. The region of interest is that section just preceding the second peak. Any evidence of positive leader propagation will show up as a slow linear rise in the electric field record. Figure 25a gives no indication of a leader. Figure 25b, though, has the characteristic ramp indicating leader propagation. Measurement of the time involved produces an approximate leader velocity of 1.7×10^7 cm/s, which is fairly consistent with the results stated previously.

Current Measurement

In addition to employing the direct method of current measurement accomplished by the I-sensor, the current flowing in the gap can also be inferred from the D-dot sensor by making a few assumptions. A simplified equivalent circuit of the experimental setup is shown in Figure 26a. Extensive ringing of the circuit was not observed in the experimental results so inductances were ignored in the circuit. The initial charging polarities of the capacitances are indicated. The circuit can be further simplified by making the following observations:

(a) Since the power supply has a relatively low output impedance, it can be considered to be fairly ideal. As such, the voltage across capacitor C_1 is essentially that of the power supply.

(b) Capacitor C_2 appears as a small impedance for the time scales of interest, enabling us to neglect the large parallel resistance, R_2.

Accordingly, the circuit of Figure 26b remains. This circuit shows that the energy necessary for flashover comes from the energy stored in the gap capacitance C_3 and directly from the power supply through capacitance C_2. Analysis of the circuit gives

$$i(t) = -C_3\, dV/dt + C_2\, d(V_1 - V)/dt \qquad (1)$$

and with V_1 = constant,

$$i(t) = -(C_3+C_2)\ dV/dt \tag{2}$$

We now assume that the gap can be modeled as a simple parallel plate capacitor with

$$V = Ed \tag{3}$$

$$D = \epsilon_o \epsilon_r E \tag{3'}$$

Since d = constant and $\epsilon_r = 1$,

$$i(t) = -(C_3+C_2)(dD/dt)d/\epsilon_o \tag{4}$$

If the D-dot sensor is placed within the uniform field region between the plates of the gap capacitor, its output will essentially give us the D-dot term contained in Equation (4). The output of the D-dot sensor is

$$V_D(t) = R_s A_s\ dD/dt \tag{5}$$

with R_s corresponding to the sensor load impedance and A_s denoting the sensor equivalent area or sensitivity. So substituting (5) into (4), we have

$$i(t) = -[(C_3+C_2)d/(\epsilon_o R_s A_s)]\ V_D(t) \tag{6}$$

This final equation provides us with a measure of the current in the gap from known constants and the output voltage of the D-dot sensor.

The accuracy of Equation (6) can be examined by comparing the signals from the D-dot sensor and the I-sensor during the same event. A typical result is shown in Figure 27. Both waveforms are displayed in the same trace, where the D-dot waveform lags the I waveform by 250 ns due to a delay line inserted in the D-dot sensor data line. Calibration of the two signals is achieved by considering total attenuation introduced in the data lines, load conditions on the lines, and Equation (6). For the I-sensor,

$$I_I(t) = (102.0)V_I(t) \tag{7}$$

and for the D-dot sensor,

$$I_D(t) = (93.1)V_D(t) \tag{8}$$

Table 1 contains a series of four measurements which are representative of the type of results achieved. The D-dot method of current measurement typically underestimates the actual measured current from the I-sensor by 8 %. This is not an unusually large discrepancy and can probably be attributed to the fact that the D-dot sensor was not located in a uniform field region or to the circuit approximations made in the calculation above.

TABLE 1
COMPARISON BETWEEN CURRENT MEASUREMENT METHODS

Arc Current, Amperes (I-sensor)	Arc Current, Amperes (D-dot Sensor)
183.60	167.58
204.00	190.86
168.30	167.58
224.40	186.20

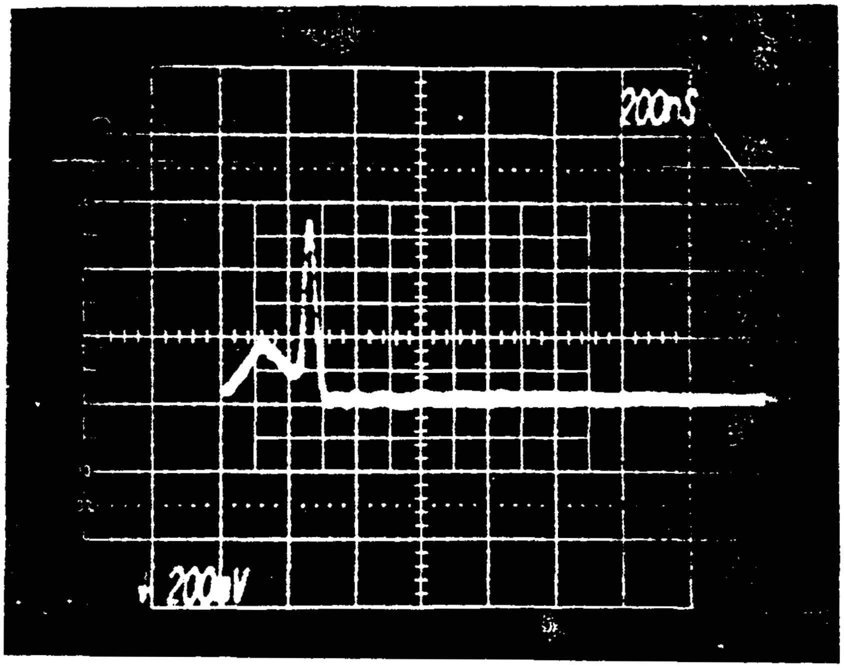

Figure 19: D-dot Response to Flashover

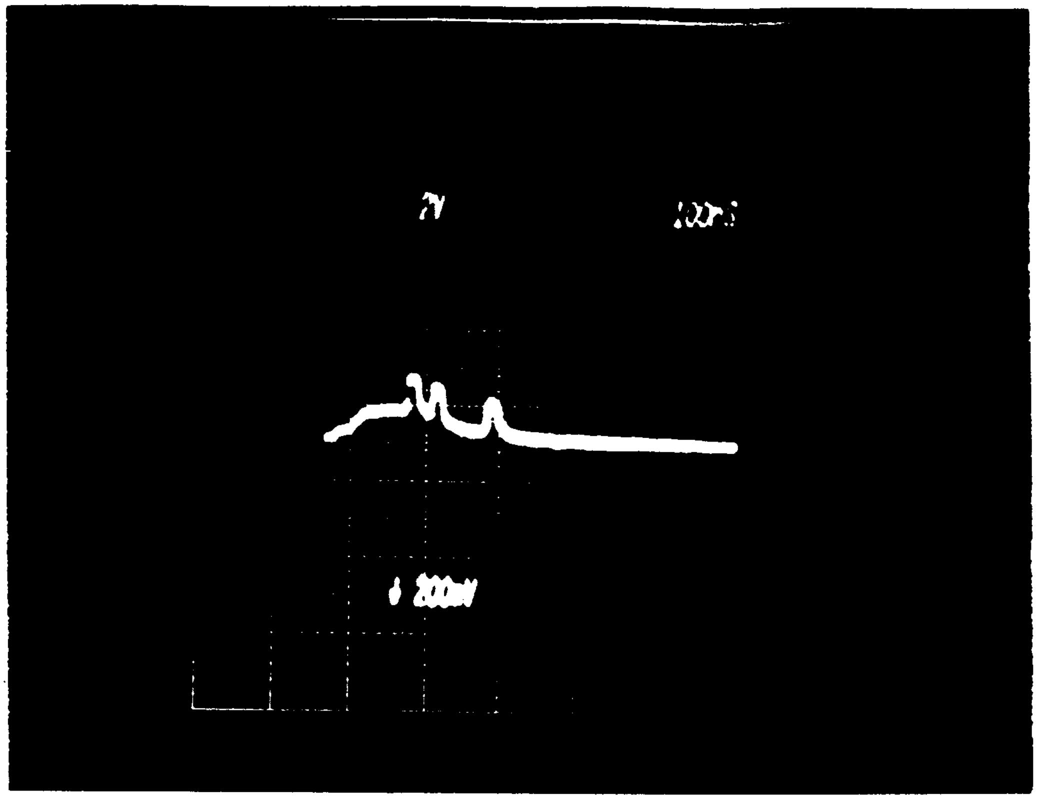

(a)

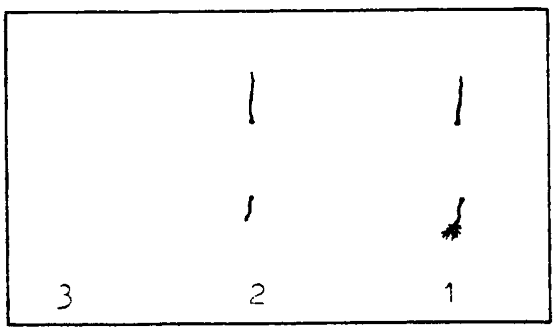

(b)

Figure 20: The First Pulse of a D-dot Waveform:
(a) Oscillogram of the first pulse with camera monitor pulses superimposed.
(b) Framing photo of the first pulse.

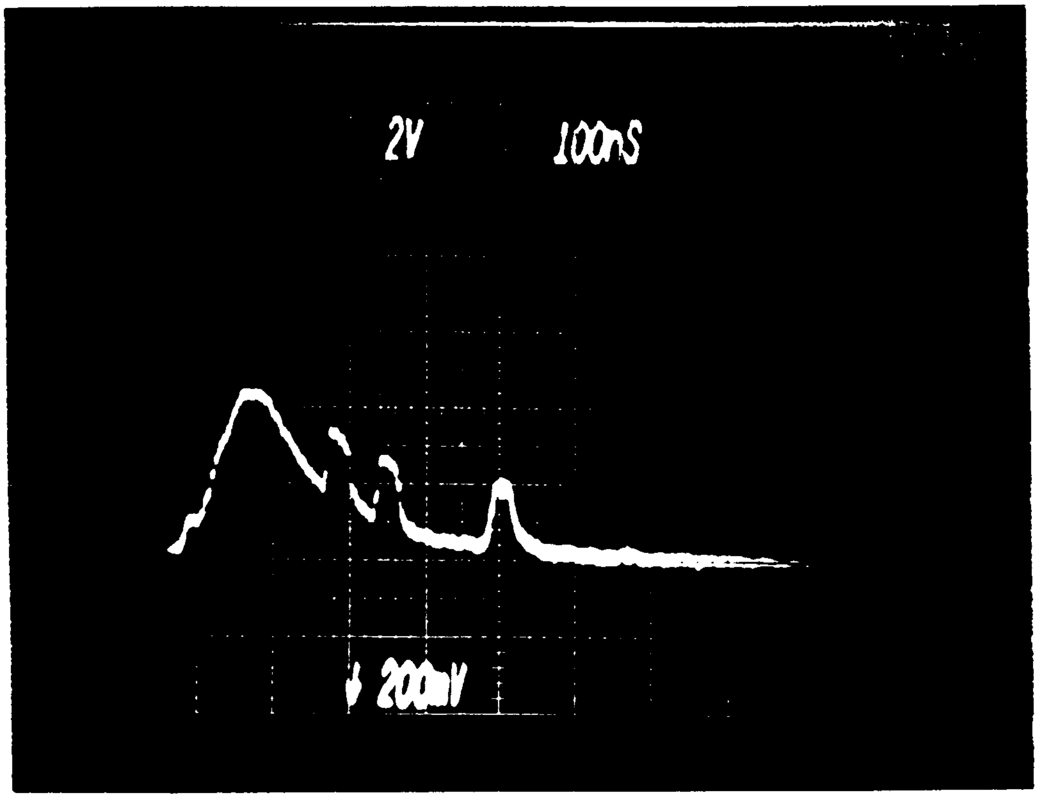

Figure 21: Fine-structure in the Leading Edge of the First Pulse of the D-dot Waveform.

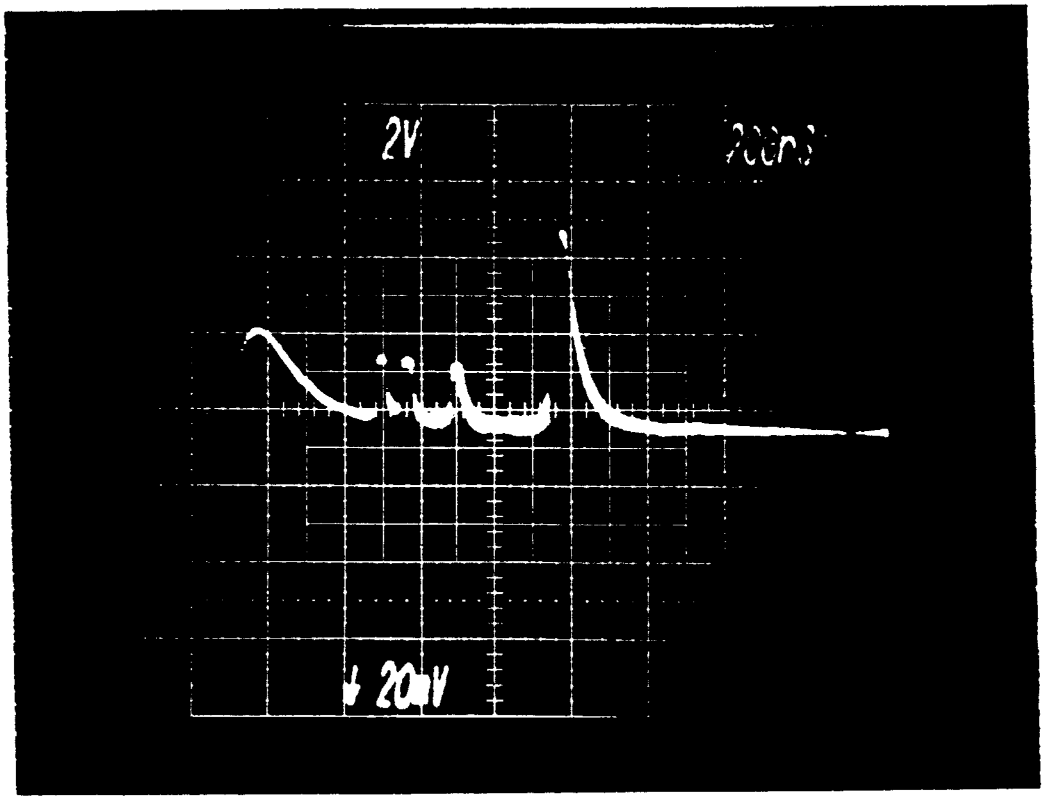

Figure 22: Oscillogram of the Extinction Period Preceding Arc Transition.

ORIGINAL PAGE IS
OF POOR QUALITY

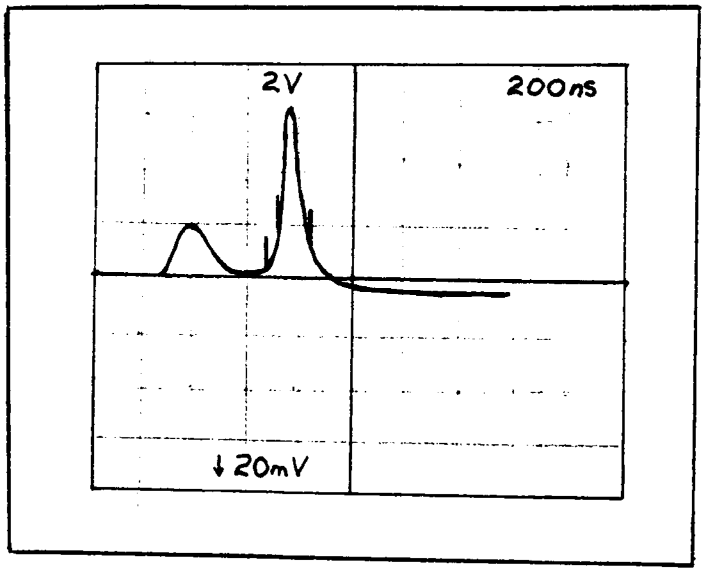

(a)

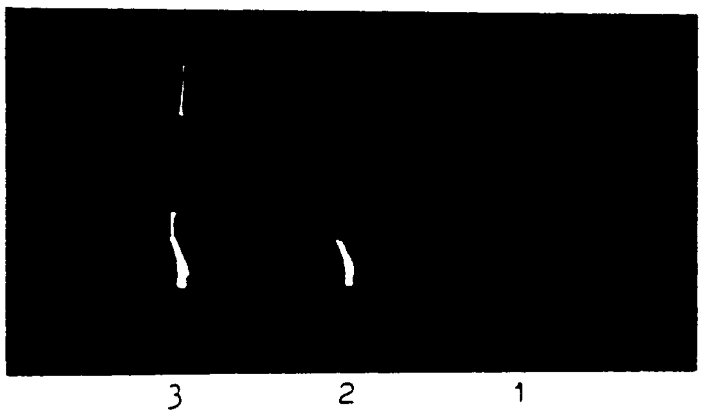

(b)

Figure 23: Transition to Arc: (a) Oscillogram with camera monitor pulses superimposed. (b) Corresponding framing photo.

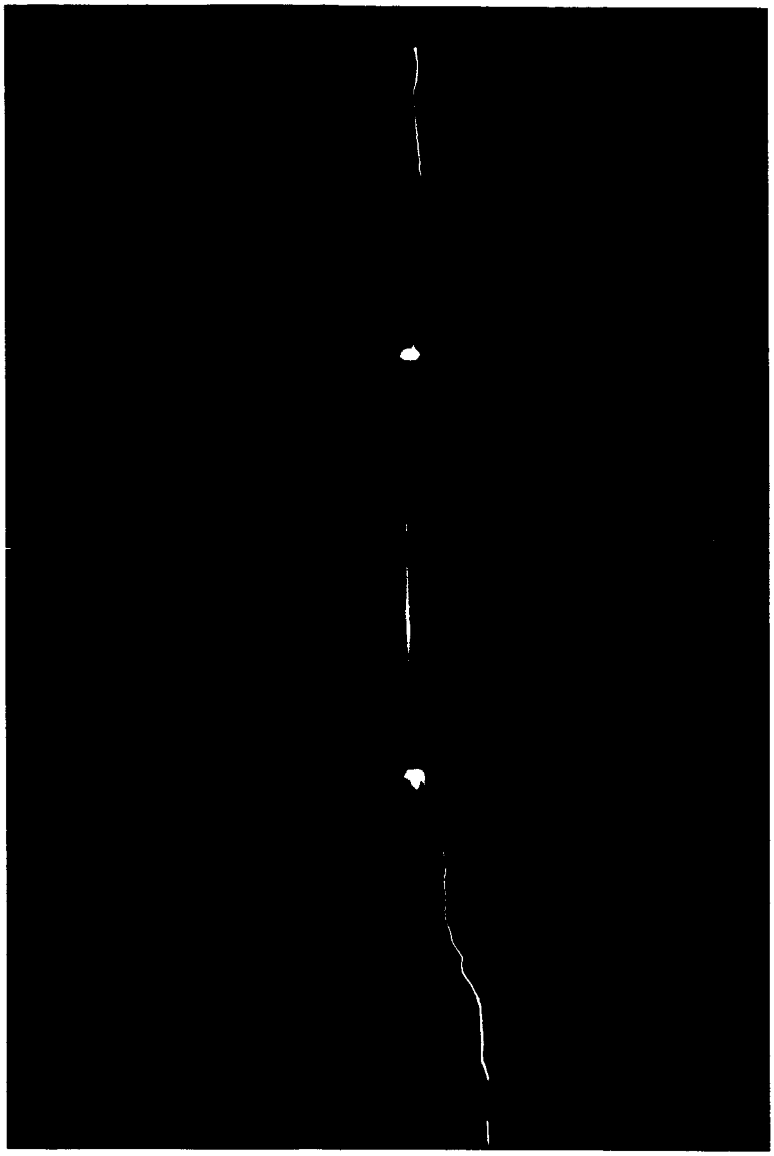

Figure 24: Color Photo of Flashover

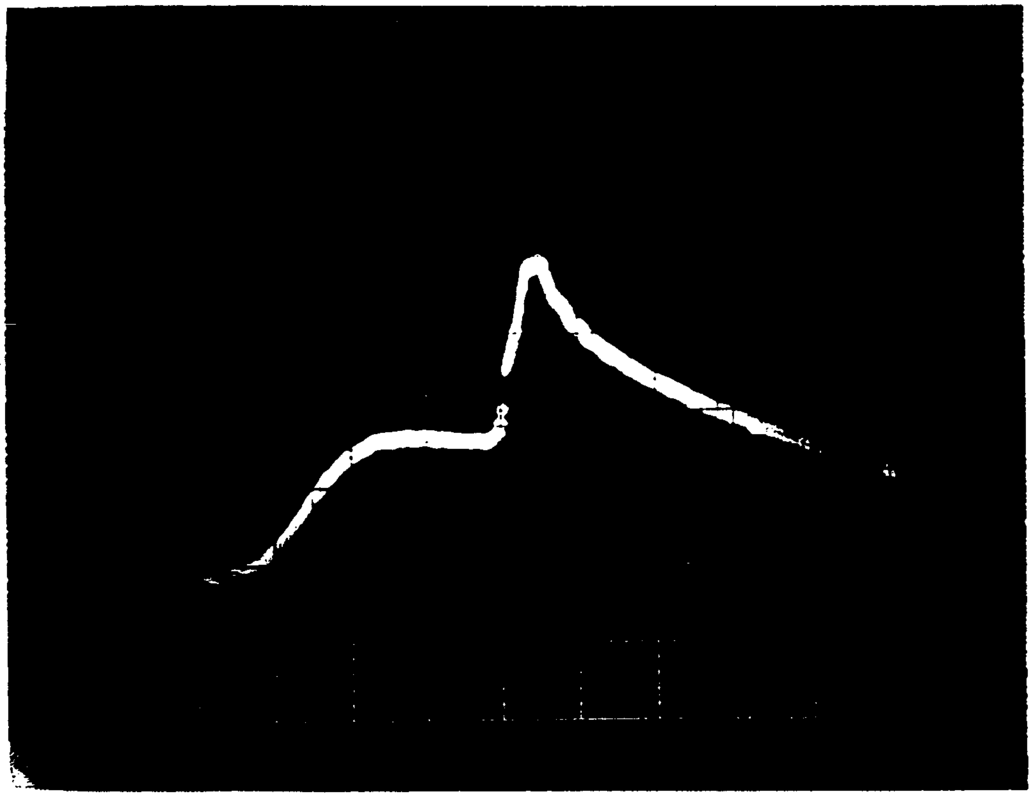

Figure 25: Integrated D-dot Waveforms of Flashover: (a) Transition to arc without leader propagation (10mV /div, 100ns/div).

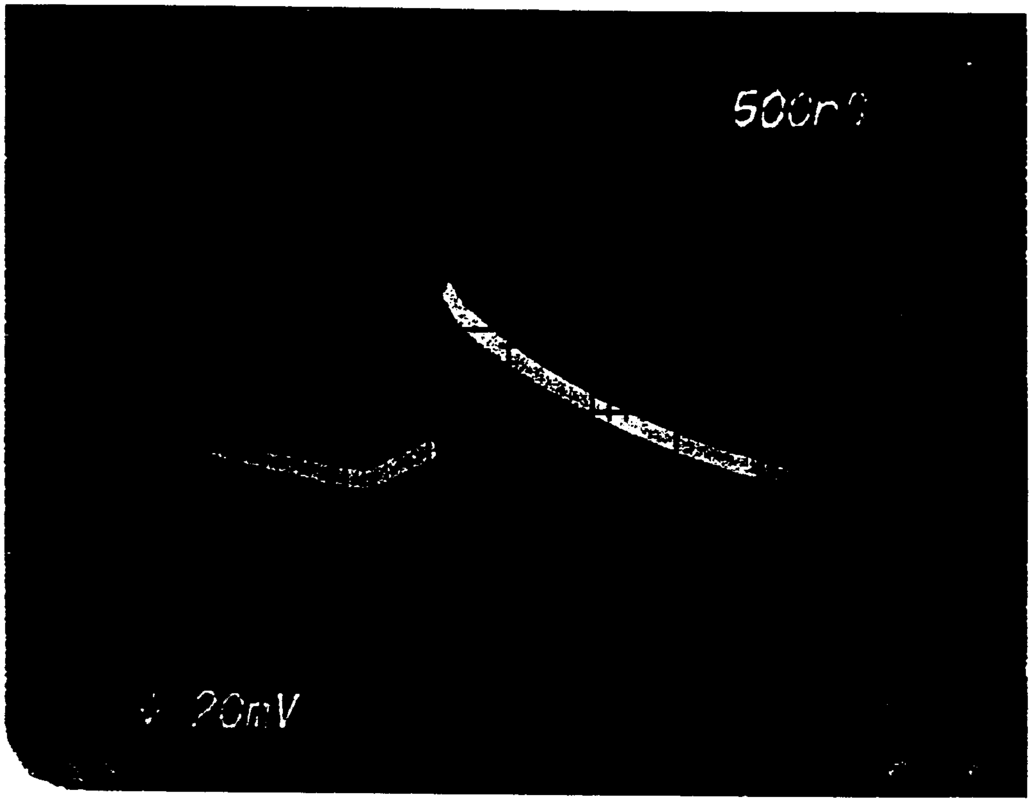

Figure 25: (Continued) (b) Transition to arc with leader propagation.

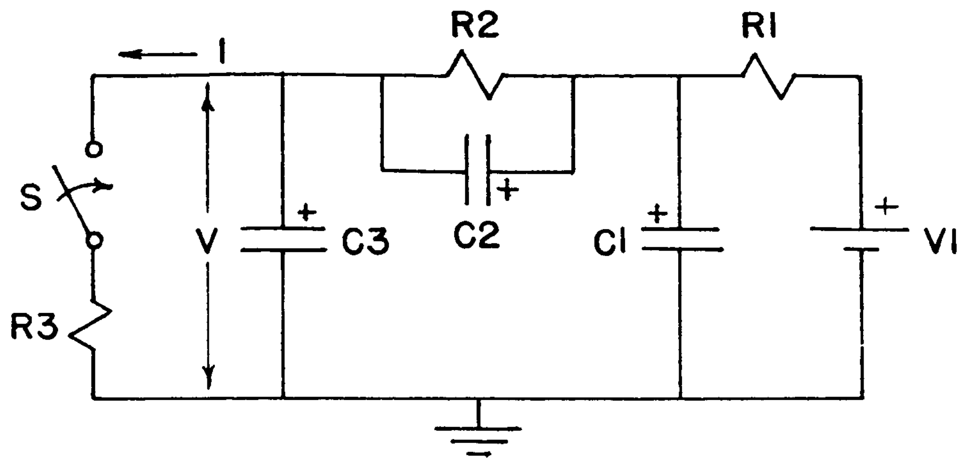

VI = POWER SUPPLY VOLTAGE
RI = POWER SUPPLY OUTPUT IMPEDANCE
CI = POWER SUPPLY CAPACITANCE
R2 = CURRENT LIMITING RESISTOR
C2 = RESISTOR—CORONA INHIBITOR STRUCTURE CAPACITANCE
C3 = GAP CAPACITANCE
R3 = GAP RESISTANCE
S = GAP BREAKDOWN

(a)

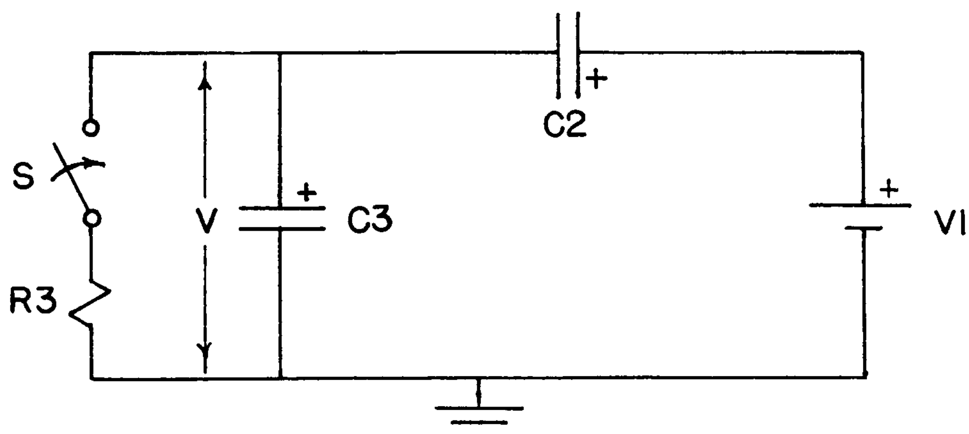

(b)

Figure 26: Equivalent Circuit of the Experimental Set-up: (a) Simple circuit representation. (b) Reduced circuit representation.

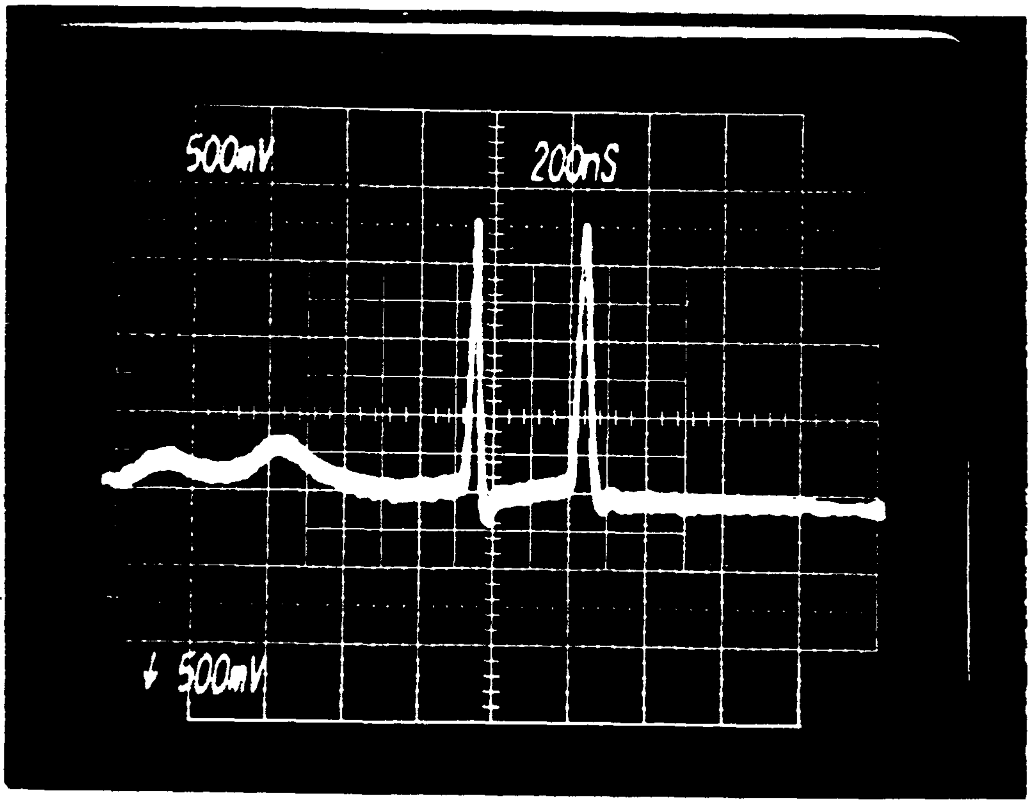

Figure 27: Simultaneous Oscillogram of Both I-sensor and D-dot Sensor Responses to Flashover (D-dot sensor response delayed by 250ns)

V. CONCLUSIONS

The individual processes involved in the breakdown of an isolated object in a uniform electric field have been examined through photographic techniques and electromagnetic sensor waveform analysis. A detailed characterization of bipolar corona was established by identifying unique properties of both positive and negative corona and their effect on subsequent arc phenomena. The negative corona remained localized near the upper tip of the ellipsoid while positive corona streamers extended from the lower tip and completely bridged the lower gap. A scenario for the flashover process was developed and can be summarized as follows:

(a) The initial phase of flashover invariably occurred in the negative point-plane (top) gap due to the shorting action of positive corona streamers traversing the entire length of the positive point-plane (bottom) gap.

(b) Connection of the ellipsoid to the high-voltage electrode by an ionized channel, or leader, in the top gap activitated the development of a positive downward leader in the bottom gap which produced a strong response at the D-dot sensor.

(c) The voltage drop caused by the current drawn through the high impedance channel of the top gap by the positive leader then produced a period of extinction in the both gaps of typically less than 1 μs.

(d) Arc transition was then initiated, causing a second strong response at the D-dot sensor. The arc occurred in one of two modes: direct transition without leader propagation in the bottom gap, and transition following leader propagation in the bottom gap. The origin of transition to arc was placed in the lower region of the bottom gap, in the manner of a lightning return stroke starting near the ground.

Two methods of current measurement were employed and tested for consistency. One method placed a sensing element directly in the current path and the other relied on using a D-dot sensor for an indirect measurement of the current. Good agreement between the two techniques was demonstrated. Peak positive corona currents were 25 mA, and peak arc currents were 200 A. From photographs, we estimate the arc channel diameter to be on the order of 0.5 mm, which gives a current density of 100 kA/cm^2--about the same as lightning.

From the results of our experiment, we can conclude that the negative point-plane gap largely determines the development of the arc. The establishment of a resistive channel in the upper gap, and resulting positive leader propagation in the lower gap, cause significant variation in the potential of the isolated object and set the gap up for a period of extinction preceding arc transition. This phenomenon is of value in the modeling of aircraft-lightning interaction. Labaune (15) and Moreau (16) have demonstrated previously that the strongest variations in the surface electric field of an isolated object occur due to current flow through this highly resistive pre-discharge channel. In addition, they have suggested a correlation between this laboratory phenomenon and data provided by instrumented aircraft. Turner (17) has found that the impedance of the attachment channel can have a profound effect on the natural resonant response of an aircraft to discharge phenomena. Further laboratory investigation of the nature of the resistive channel preceding arc transition, therefore, is certainly warranted. It is also interesting to note that the relaxation process described in (a)-(c) above is very similar to that observed in the large-gap experiments of Labaune (15) and Moreau (16).

It is known that the presence of rain will substantially lower the flashover voltage of a negative point-plane gap but not that of a positive point-plane gap (18). Brief tests in our experimental set-up where a fine water mist was injected into the gap showed that a large drop in flashover voltage was obtained. This merits detailed examination in the future since here different processes may come into play, with the negative point-plane gap no longer controlling the breakdown process.

Improvements in our present experimental set-up might consist of the addition of water and air motion to the gap, order of magnitude increase in the gap dimension, and the inclusion of streak photography in the data acquisition system. An attempt should be made to measure the time-dependent impedance of predischarge ionized channels, or leaders, which form in the gap. The use of isolated objects of different shapes is also of importance.

The behavior of the leaders is especially interesting because it is probably the main distinguishing factor between aircraft-triggered lightning strikes and aircraft-intercepted strikes. To study this behavior further in the laboratory, a much larger gap is needed, so that the leaders can develop freely without contacting the electrodes. The key question seems to be, "what are the conditions needed to obtain a propagating leader from an isolated body?"

§

REFERENCES

1. Pitts, F. "Electromagnetic Measurement of Lightning Strikes to Aircraft," Journal of Aircraft, vol. 19, no. 3, Mar. 1982, pp. 246-250.

2. Trost, T. "Interpretation of a Class of In-flight Lightning Signatures," Proc. Intl. Aerospace and Ground Conf. on Lightning and Static Electricity, Dayton, OH, June 1986, pp. 6-1, 6-9.

3. Rudolph, T., et al. "Development and Application of Linear and Nonlinear Methods for Interpretation of Lightning Strikes to In-Flight Aircraft," NASA CR 3974, Sept. 1986.

4. Mazur, V., et al. "Conditions Conducive to Lightning Striking an Aircraft in a Thunderstorm," Proc. Intl. Aerospace and Ground Conf. on Lightning and Static Electricity, Ft. Worth, TX, June 1983, pp. 90-1, 90-7.

5. Cesani, J. "Flashover Test of an Isolated Conducting Object in a 10-inch Gap," Master's Thesis, Texas Tech Univ., Dec. 1985.

6. Hutzler, B., et al. "High Voltage Laboratory Test and Lightning Phenomena," Proc. Intl. Aerospace and Ground Conf. on Lightning and Static Electricity, Paris, France, June 1985, pp. 191-196.

7. Levesque, P., et al. "A Study of the Physical Mechanism and Perturbations Created by the Attachment of an Arc to a Conducting Cylinder," Proc. Intl. Aerospace and Ground Conf. on Lightning and Static Electricity, Paris, France, June 1985, pp. 29-36.

8. Baum, C., et al. "Sensors for Electromagnetic Pulse Measurements Both Inside and Away From Nuclear Source Regions," IEEE Transactions on Antennas and Propagation, vol. AP-26, no. 1, Jan. 1978, pp. 26-27.

9. Baum, C., ed. "Electromagnetic Pulse Sensor Handbook," EMP Measurement, vol. 1-1, sec. 3, June 1971.

10. Latham, R., and Lee, K. "Capacitance and Equivalent Area of a Disk in a Circular Aperture," Sensor and Simulation Note, no. 106, May 1970.

11. Nasser, E. Fundamentals of Gaseous Ionization and Plasma Electronics, Wiley-Interscience, New York, 1971, pp. 329-330.

12. Bicknell, J., and Humood, B. "The Streamer to Spark Transition," Proc. Intl. Aerospace and Ground Conf. on Lightning and Static Electricity (Appendum), Ft. Worth, TX, June 1983, pp. 42-1, 42-6.

13. Nasser, E. Fundamentals of Gaseous Ionization and Plasma Electronics, Wiley-Interscience, New York, 1971, p. 346.

14. Bicknell, J., and Humood, B. "Bipolar Corona and Aircraft-Triggered Discharges," Proc. Intl. Aerospace and Ground Conf. on Lightning and Static Electricity, Orlando, FL, June 1984, pp. 4-1, 4-4.

15. Labaune, G., et al. "Experimental Study of the Interaction Between an Arc and an Electrically Floating Structure," Proc. Intl. Aerospace and Ground Conf. on Lightning and Static Electricity, Dayton, OH, June 1986, pp. 27-1, 27-9.

16. Moreau, J., and Alliot, J. "Analysis of the First Milliseconds of Aircraft Lightning Attachment," Proc. Intl. Aerospace and Ground Conf. on Lightning and Static Electricity, Paris, France, June 1985, pp. 18-1, 18-6.

17. Turner, C., and Trost, T. "Laboratory Modeling and Analysis of Aircraft-Lightning Interaction," NASA CR 169455, Aug. 1982.

18. Knudson, N., et al. "Flashover Test on Large Gaps with DC Voltage and with Switching Surges Superimposed on DC Voltage," IEEE Trans. Power Apparatus and Systems, vol. PAS-89, no. 5/6, May/June 1970, pp. 781-788.

APPENDIX

A certain amount of delay is present in our Image Converter Camera trigger system. As mentioned earlier, the Trigger Delay Generator (TDG) is responsible for producing the 300 V pulse needed to trigger the camera. The trigger input of the TDG has a minimum threshold of 1 V. The gate output of the scope will deliver, at best, only 1 V into the 50 ohm load presented by the trigger input, or 10 V if the load is 1 megohm. Therefore, a high-speed JFET source-follower amplifier was added to the gate output of the scope. With this addition, the gate voltage transferred to the TDG was well above the 1 V threshold and thus more reliable triggering was obtained. To insure minimum trigger delay, all cable lengths were minimized. Unfortunately, the TDG has a measured internal delay of 115 ns, which is much higher than its 50 ns rated value. (We did not have time to repair or modify the TDG.) Adding up all of the delays in the system yields an "event-to-photo" delay of approximately 150 ns. As such, we are rather limited in how quickly we can photograph an event.

Standard Bibliographic Page

1. Report No. NASA CR-178323	2. Government Accession No.	3. Recipient's Catalog No.
4. Title and Subtitle Breakdown Characteristics of an Isolated Conducting Object in a Uniform Electric Field		5. Report Date December 1986
		6. Performing Organization Code
7. Author(s) M. G. Grothaus and T. F. Trost		8. Performing Organization Report No.
9. Performing Organization Name and Address Dept. of Electrical Engineering/Computer Science Texas Tech University Lubbock, TX 79409		10. Work Unit No. 505-66-21-04
		11. Contract or Grant No. NAG-1-28
12. Sponsoring Agency Name and Address National Aeronautics and Space Administration Washington, DC 20546-0001		13. Type of Report and Period Covered Contractor Report 1984-1986
		14. Sponsoring Agency Code
15. Supplementary Notes Langley Technical Monitor: Felix L. Pitts		

16. Abstract

A laboratory experiment has been conducted to determine the physical processes involved in the electrical breakdown of a particular spark gap arrangement. The gap consists of an isolated conducting ellipsoid located midway between two large flat electrodes. Gradual increase of the applied electric field, E, in the gap produces corona on the ellipsoid tips followed by flashover in a leader-arc sequence. The leader phase consists of the abrupt formation of ionized channels which partially bridge the gap and then decay prior to the arc. Measurements of dE/dt and of current were made, and photographs were taken with an image converter camera.
Experimental parameters are as follows:

Gap length = 25.4 cm
Ellipsoid length = 10.0 cm
Gap voltage for flashover = 98 kV
Gap electric field strength (far from ellipsoid) = 386 kV/m
Gap capacitance = 78 pF
Gap electric field energy (estimated) = 0.58 J
Peak positive-corona-streamer current = 25 mA
DC corona current = 0.37 - 0.40 mA
Peak arc current = 200 A
Arc channel diameter < 1 mm
Duration of flashover event (leader + arc) $\simeq 1\ \mu s$.

17. Key Words (Suggested by Authors(s)) Electrical breakdown processes Laboratory experiment Lightning Spark gaps Image converter camera		18. Distribution Statement Unclassified-Unlimited Subject category 47	
19. Security Classif.(of this report) Unclassifed	20. Security Classif.(of this page) Unclassified	21. No. of Pages 66	22. Price A04